Biophysical Journal
Article

Biophysical Society

Role of Pore-Lining Residues in Defining the Rate of Water Conduction by Aquaporin-0

Patrick O. Saboe,[1] Chiara Rapisarda,[2] Shreyas Kaptan,[3] Yu-Shan Hsiao,[2] Samantha R. Summers,[1] Rita De Zorzi,[2] Danijela Dukovski,[2] Jiaheng Yu,[1] Bert L. de Groot,[3] Manish Kumar,[1,*] and Thomas Walz[2,*]
[1]Department of Chemical Engineering, Pennsylvania State University, University Park, Pennsylvania; [2]Department of Cell Biology, Harvard Medical School, Boston, Massachusetts; and [3]Computational Biomolecular Dynamics Group, Max Planck Institute for Biophysical Chemistry, Göttingen, Germany

ABSTRACT Compared to other aquaporins (AQPs), lens-specific AQP0 is a poor water channel, and its permeability was reported to be pH-dependent. To date, most water conduction studies on AQP0 were performed on protein expressed in *Xenopus* oocytes, and the results may therefore also reflect effects introduced by the oocytes themselves. Experiments with purified AQP0 reconstituted into liposomes are challenging because the water permeability of AQP0 is only slightly higher than that of pure lipid bilayers. By reconstituting high amounts of AQP0 and using high concentrations of cholesterol to reduce the permeability of the lipid bilayer, we improved the signal-to-noise ratio of water permeability measurements on AQP0 proteoliposomes. Our measurements show that mutation of two pore-lining tyrosine residues, Tyr-23 and Tyr-149 in sheep AQP0, to the corresponding residues in the high-permeability water channel AQP1 have additive effects and together increase the water permeability of AQP0 40-fold to a level comparable to that of AQP1. Molecular dynamics simulations qualitatively support these experimental findings and suggest that mutation of Tyr-23 changes the pore profile at the gate formed by residue Arg-187.

INTRODUCTION

The function of the ocular lens, which consists of concentrically organized fiber cells, is to focus incoming light onto the retina at the back of the eye. To serve this function, the lens must be transparent and be able to change its shape so the eye can focus on objects at different distances, a process known as accommodation. The shape changes of the lens needed for accommodation are accompanied by changes in the volume of the fiber cells, which therefore depend on a highly water-permeable membrane (1).

Aquaporin-0 (AQP0), a member of the ubiquitous AQP family, is a water channel that is exclusively expressed in the lens, where it is the most abundant membrane protein (2). AQP0 is highly specialized to the needs of the lens. In addition to making the fiber cell membrane water permeable, which is necessary to enable circular solute flow in the lens (1) and to allow for the volume changes in the fiber cells that accompany accommodation, AQP0 is involved in the formation of membrane junctions and thus helps to maintain the cell architecture of the lens and minimize extracellular gaps between the fiber cells (1,3–6). The importance of AQP0 for lens homeostasis is illustrated by the fact that mutations in AQP0 result in cataract formation (7).

In addition to being involved in membrane junction formation, AQP0 is also an unusual member of the AQP family in that it has very poor water permeability. When AQP0 is expressed in *Xenopus* oocytes, its water permeability is ~40 times lower than that of AQP1, a water channel found in red blood cells and the kidney (8). The low water

Submitted November 7, 2016, and accepted for publication January 26, 2017.

*Correspondence: manish.kumar@psu.edu or twalz@mail.rockefeller.edu

Patrick O. Saboe, Chiara Rapisarda, and Shreyas Kaptan contributed equally to this work.

Patrick O. Saboe's present address is National Renewable Energy Laboratory, Golden, Colorado.

Chiara Rapisarda's present address is Institut Pasteur, Paris, France.

Shreyas Kaptan's present address is Department of Physics and Earth Sciences, Jacobs University, Bremen, Germany.

Yu-Shan Hsiao's present address is Metabolism Program, Broad Institute, Cambridge, Massachusetts.

Samantha R. Summers's present address is Department of Chemical and Biological Engineering, University of Colorado, Boulder, Colorado.

Rita De Zorzi's present address is Dipartimento di Scienze Chimiche e Farmaceutiche, Università degli Studi di Trieste, Trieste, Italy.

Danijela Dukovski's present address is Proteostasis Therapeutics, Cambridge, Massachusetts.

Thomas Walz's present address is Laboratory of Molecular Electron Microscopy, Rockefeller University, New York, New York.

Editor: Andreas Engel.

http://dx.doi.org/10.1016/j.bpj.2017.01.026

permeability of mammalian AQP0 was previously proposed to minimize the destabilization of AQP0-mediated membrane junctions as a result of high water flows (9) or, alternatively, to represent an adaptation of air-living organisms to a dry environment (10). The structure of AQP0 has been determined by both electron and x-ray crystallography (11–13). A comparison of the AQP0 structure with those of other AQPs revealed differences in the pore-lining residues that could explain its low water permeability. In particular, the side chains of two tyrosine residues, Tyr-23 and Tyr-149, in sheep AQP0 extend into the water pathway, obstructing water molecules permeating the channel (Fig. 1, *A* and *B*). In AQP1, these tyrosine residues are substituted by Phe-24 and Thr-157, respectively, which have smaller side chains than Tyr-23 and Tyr-149 (Fig. 1 *B*). Molecular-dynamics (MD) simulations implicated these two tyrosine residues in the reduced water permeability of AQP0 (9,14,15), but this notion has not been tested experimentally.

Another characteristic of AQP0-mediated water conduction is its pH sensitivity (16–18), although this behavior has not been observed in all studies (19,20). In permeability studies with AQP0 expressed in *Xenopus* oocytes, water conduction was reported to be two to four times higher at pH 6.5 than at higher or lower pH values (16–20). A comparison of the sequence of AQP0 with AQP1, which is not pH sensitive, identified a histidine residue in AQP0, His-40 (Fig. 1 *C*), that is not present in AQP1 and thus is a likely candidate to be the pH sensor in AQP0. An effect of this residue on pH-dependent water conduction was corroborated by mutations at or near the residue (16,17). However, structures of AQP0 determined at pH 6 and pH 10 by means of electron (13) and x-ray crystallography (12), respectively, showed no significant differences in the conformation of residues His-40 and His-66, the two residues that are most likely to respond to pH changes. Hence, whether AQP0 water conduction is indeed affected by pH, how it is affected, and the mechanism underlying pH regulation remain open questions.

Here, we expressed AQP0 variants in the yeast *Pichia pastoris* and reconstituted the recombinant protein into proteoliposomes for stopped-flow measurements of water conduction. To optimize the accuracy of the measurements, the vesicles were formed with a very low lipid/protein ratio (LPR) of 2 (mg/mg) to maximize AQP0-mediated water conduction, and the lipid composition of the vesicles was optimized to minimize water leakage through the lipid bilayer. Our measurements show that the low permeability of AQP0 for water is predominantly due to Tyr-23, with Tyr-149 making a smaller contribution. Substitution of both tyrosine residues by the corresponding ones in AQP1 raised the water permeability of AQP0 to the level of that of AQP1. MD simulations performed in parallel are consistent with the experimental results, showing that both mutations increase water conduction, with mutation of Tyr-23 having a greater effect. We also found that AQP0-mediated water conduction is only mildly pH sensitive, with a modest increase in water permeability by a factor of 1.5–2 at pH 7.5 compared with that at pH 6.5. Mutation of His-40 and His-66 seems to further reduce the already low pH dependence of AQP0 water conduction.

MATERIALS AND METHODS

Materials

n-Octyl-β-D-glucoside (OG) was purchased from Affymetrix (Santa Clara, CA). Brain phosphatidylserine (PS), chicken egg phosphatidylcholine (PC), chicken egg phosphatidylglycerol (PG), *Escherichia coli* polar lipids (EPL), dimyristoyl phosphatidylcholine (DMPC), dioleoyl

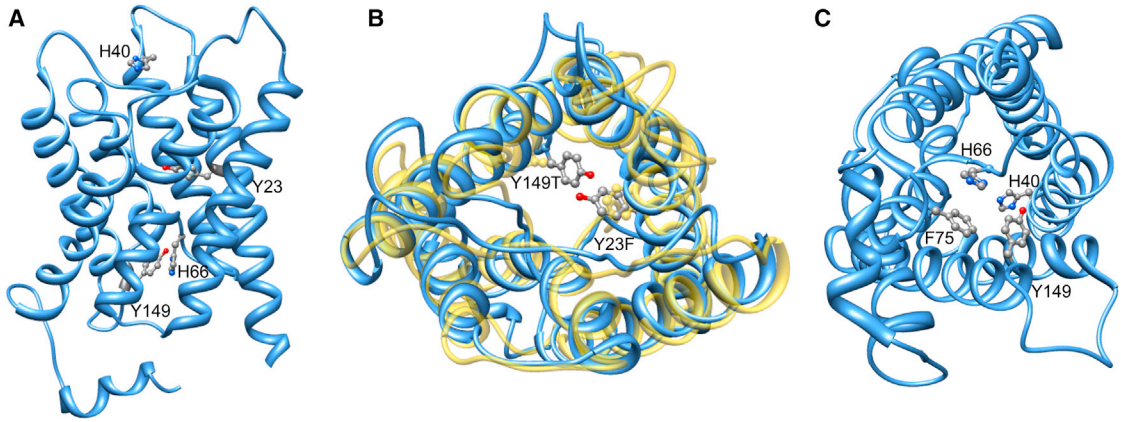

FIGURE 1 Pore-lining residues implicated in the low water permeability of AQP0. (*A*) Ribbon diagram of AQP0 viewed parallel to the membrane plane. Residues that were evaluated in this study are labeled and shown in stick representation. (*B*) Tyrosine residues 23 and 149 (shown in *gray* with *red* hydroxyl groups) extend into the water pathway and have been implicated in the low water permeability of AQP0 (shown as *blue* ribbon diagram). In the high-permeability water channel AQP1 (shown in *yellow*), these two tyrosine residues are substituted by residues with smaller side chains (Tyr-23 by phenylalanine and Tyr-149 by threonine). (*C*) Ribbon diagram of AQP0 viewed perpendicular to the membrane plane. Residues proposed to play a role in the pH modulation of AQP0 water permeability are His-40 at the extracellular entrance of the pore, and His-66, which is part of constriction site II, formed by Phe-75, His-66, and Tyr-149, at the cytoplasmic entrance of the pore. Note: (*B*) and (*C*) present two different views of the protein. To see this figure in color, go online.

phosphatidylethanolamine (DOPE), and cholesterol (Chl) were purchased from Avanti Polar Lipids (Alabaster, AL). Talon metal affinity resin was obtained from Clontech Laboratories (Mountain View, CA), restriction enzymes were obtained from New England Biolabs (Ipswich, MA), and zeocin was obtained from Invitrogen (Grand Island, NY).

Purification of native AQP0

Native AQP0 was purified from sheep lenses as previously described (21). Briefly, membranes prepared from the lens cortex were solubilized with 4% OG in 10 mM Tris (pH 8) for 1 h at 4°C. After centrifugation at 300,000 × *g* for 30 min, the supernatant was applied to a MonoQ column (Amersham, Little Chalfont, UK) equilibrated with 1.2% OG in 10 mM Tris (pH 8), and AQP0 was eluted with 300 mM NaCl in the same buffer. AQP0-containing fractions were pooled and run over a Superose 12 column (Amersham) equilibrated with 1.2% OG in 10 mM Tris (pH 8) and 100 mM NaCl.

Plasmids

Both strands of the sheep AQP0 cDNA (codon optimized for yeast) with XhoI and *Eco*RI ends were synthesized and cloned into a picZ plasmid that was engineered with a PreScission (PPX) cutting site before the C-terminal His_{10} tag. Point mutations in the sheep AQP0 sequence were introduced by PCR using the primers listed in Table 1. Clones containing the mutations were selected and confirmed by sequencing with the 3AOX and 5AOX primers provided by the sequencing platform.

Expression of AQP0 in *P. pastoris*

picZ plasmids containing genes for wild-type AQP0 (wtAQP0) and mutant AQP0 were linearized with PmeI and transformed by electroporation into the protease-deficient *P. pastoris* strain SMD1163. Transformants that had the plasmid incorporated into the genome were selected on YPDS plates containing 1 mg/mL zeocin. Single colonies from the plates were expanded to 50-mL cultures in YPD medium and grown overnight at 30°C. The precultures were transferred to YNB-based glycerol-containing medium (BMG) and incubated for 24 h at 30°C with shaking at 250 rpm. After the exponential growth phase, the growth medium was exchanged with expression-inducing medium containing 0.5% methanol (BMM). After 24 h at 28°C, cells were harvested by centrifugation, washed with deionized water, flash-frozen in liquid nitrogen in small pellets, and stored at −80°C.

Purification of AQP0 from *P. pastoris*

Cell pellets were cooled in liquid nitrogen and ground five times for 3 min in a mixer mill (MM400, Retsch, Haan, Germany) at a frequency of 25 beats/s. The fine powder was resuspended with lysis buffer containing 50 mM Tris (pH 7.4), 150 mM NaCl, and 0.5 mL/50 mL Halt protease inhibitor cocktail (Pierce, Dallas, TX). The cells were then mixed with an equal volume of 0.5-mm glass beads and subjected to 10 cycles of 10 s mix and 50 s pause using a modified blender (Biospec, Bartlesville, OK) at 0°C. After centrifugation at 4000 × *g* for 15 min to remove unbroken cells, the membranes were pelleted by centrifugation at 200,000 × *g* for 1 h and solubilized with 25 mL of 4% OG in 20 mM Tris (pH 8) and 300 mM NaCl. After centrifugation at 200,000 × *g* for 30 min, the supernatant was incubated with 1/25 volume of Talon metal affinity resin (Clontech, Mountain View, CA) in equilibration buffer (1.2% OG, 20 mM Tris (pH 8) and 300 mM NaCl) for 1 h at 4°C. The resin was washed with 25 volumes of 20 mM imidazole and five volumes of 60 mM imidazole in equilibration buffer. AQP0 was eluted using two volumes of 500 mM imidazole in equilibration buffer. Buffer exchange was performed using a 10DG desalting column (Biorad, Hercules, CA) to remove the imidazole and to supplement the equilibration buffer with 1 mM dithiothreitol. The C-terminal His_{10} tag was removed by incubation with His-tagged PPX-3C protease (1:10 mg/mg) for 16 h (22), and the PPX was removed by gel filtration with a Superose 12 column (Amersham) in gel-filtration buffer (1.2% OG, 10 mM Tris (pH 8.0), 100 mM NaCl). Complete removal of the tag was confirmed by Western blotting with anti-His antibody.

Formation of lipid vesicles and AQP0 proteoliposomes

Before they were reconstituted into proteoliposomes, the AQP0-containing fractions from the gel-filtration column were pooled and concentrated, and the protein concentration was determined via a Bradford assay (Pierce) using bovine serum albumin as the protein standard. Purified AQP0 was reconstituted into proteoliposomes by dialysis. AQP0 (0.5 mg/mL in reconstitution mixture) was mixed with OG-solubilized PS/PC/Chl (1:4:5 mol/mol/mol) at an LPR of 2 (mg/mg), and the volume was adjusted to 0.5 mL with gel-filtration buffer. The mixtures were transferred to dialysis cassettes (3.5 kDa cutoff; Pierce) and dialyzed against buffer containing 20 mM MES (pH 6.5) or 20 mM HEPES (pH 7.5) with 100 mM NaCl and 0.5% (w/V) NaN_3 for 3 days at 4°C with daily buffer exchanges. Pure liposomes were formed using the same method at a lipid concentration of 1 mg/mL. Proteoliposomes and liposomes were harvested and extruded 20 times through a 0.2 μm membrane. The size of the vesicles was measured by dynamic light scattering (Viscotek TDA model 302 or Malvern Zetasizer Nano ZS; Malvern, UK).

Permeability measurements

The permeability of liposomes and proteoliposomes containing native AQP0 or recombinant wtAQP0 or mutant AQP0 was calculated from light-scattering intensity data measured with a stopped-flow apparatus (either an SF-E100 or SF-300X machine; KinTek, Austin, TX) as previously described (23). Shrinkage of both liposomes and proteoliposomes was initiated with 400 mOsm NaCl at 15°C. Results are the average of a minimum of 10 traces obtained with at least three independent vesicle batches.

MD simulations

For the MD simulations, we used the 1.9 Å resolution electron crystallographic structure of AQP0 (PDB: 2B6O) (11). Using CHARMM-GUI (24),

TABLE 1 Primers Used to Introduce Point Mutations in Sheep AQP0

Mutation	Forward Primers	Reverse Primers
Y23F	5′-TTC GCA ACT TTG TTT TTT GTT TTC TTT GGT TTG-3′	5′-CAA ACC AAA GAA AAC AAA AAA CAA AGT TGC GAA
Y149T	5′-TGT ATC TTC GCT ACT TAC GAT GAA AGA AGA AAT-3′	5′-ATT TCT TCT TTC ATC GTA AGT AGC GAA GAT ACA-3′
H40Q	5′-GCA CCA GGT CCT TTG CAA GTT TTA CAA GTT GCT-3′	5′-AGC AAC TTG TAA AAC TTG CAA AGG ACC TGG TGC-3′
H66M	5′-GGT CAT ATT TCT GGT GCA ATG GTT AAT CCT GCT GTT ACC-3′	5′-GGT AAC AGC AGG ATT AAC CAT TGC ACC AGA AAT ATG ACC-3′

Underline indicates the mutation sites.

this structure was embedded into a membrane bilayer consisting of 365 1-palmitoyl-2-oleoyl-*sn*-glycero-3-phosphocholine (POPC) molecules. The water box surrounding the membrane contained 150 mM NaCl. The parameters for the protein, lipids, ions, and water were obtained from the CHARMM36 force field (25). Standard CHARMM cutoffs for electrostatic and van der Waals interactions of 1 nm were used in the simulations. Electrostatics was treated with the particle mesh Ewald method (26). For the final production runs, the v-rescale thermostat (27) was set to a temperature of 305 K (room temperature) and the Parrinello-Rahman barostat was set to a pressure of 1 atm to maintain an NPT ensemble. All simulations were performed with the GROMACS 5.0 package (28). All proteins (wtAQP0 and the Y23F, Y149T, and Y23F/Y149T mutants) were simulated for 500 ns each. The first 100 ns were considered the equilibration time, and the remaining 400-ns trajectories were used for analysis. In addition, 300-ns simulations were performed for 14 additional mutations that were thought to increase the AQP0 water permeability. The water permeability was calculated from the MD simulations by means of the collective-diffusion method (29).

Functional mode analysis

The trajectories from the MD simulations were analyzed with the machine learning algorithm, partial least-square-based functional mode analysis (PLS-FMA) (30,31). In an approach similar to that described in our previous work (32), the protein was divided into four equal regions along the channel axis (see Fig. 5 and Fig. S8 in the Supporting Material). The program HOLE (33) was then used to calculate the minimum radius along the channel axis for each of the four regions for the simulation trajectories, yielding four independent data vectors. Each of these vectors was divided into two equal parts, with the first one used to train the PLS-FMA model and the second one used for validation. The PLS-FMA methodology was then used to generate a model from the training set that predicted the structural changes in the protein that best correlated with the changes in the data vector. A correlation coefficient of >0.75 in the validation set was considered to be statistically significant for further analysis (Fig. S8). Fifteen PLS components were used to predict the collective modes from the data (the use of more components led to overfitting). Only three of the four regions yielded statistically significant modes. In the region ranging from -16 to -8 Å, no collective motion correlated highly with changes in the minimum radius. All modes were computed over the entire trajectories without any bias in the process.

Essential-dynamics simulations

Essential-dynamics (ED) simulations were carried out using the make_edi tool implemented in GROMACS 5.0 (34). These simulations were used to restrain the protein in the open and closed states of the arginine gate mode with a harmonic constraint of 1000 kJ/mol^{-1} nm^{-1}. Simulations were carried out for 100 ns for wtAQP0 and the Y23F mutant in each state.

RESULTS

Water permeability of wtAQP0

The water permeability of pure lipid bilayers ranges from 10 to 150 μm/s depending on the lipid composition and temperature (35). We used dialysis and extrusion to form liposomes composed of DMPC, EPLs, and mixtures of egg PC and egg PG. Stopped-flow measurements were conducted at a pH of 6.5 and a temperature of 15°C (25°C for DMPC due to its high phase transition temperature of 24°C). The measured water permeability values of DMPC, PC/PG, and EPL vesicles were 14.7 ± 2.3, 21.2 ± 4.3, and 16.4 ± 1.4 μm/s, respectively (Figs. S1–S3; Table S1). Incorporation of AQP0 increased the permeability of DMPC, PC/PG, and EPL vesicles by only a factor of ~2–3.5, even at very high protein concentrations (i.e., at LPRs as low as 2 (mg/mg)), which made it difficult to discern the contribution of AQP0 to the total water permeability of the proteoliposomes (Figs. S1–S3; Table S1).

It is known that addition of Chl decreases the water permeability of lipid bilayers (35). To determine the effect of Chl, we prepared PC/PG (4:1 mol/mol) and PC/PG/Chl (2:1:2 mol/mol/mol) mixtures according to the mixing ratios used in a previous AQP0 water permeability study by Tong et al. (36) (Figs. S4 and S5; Table S2). In addition, a PC/PS/Chl (4:1:5 mol/mol/mol) mixture (Fig. S6) was prepared in accordance with the lipid mixture that was used by Itel et al. (37) to reduce the gas permeability of lipid vesicles in a study of the CO_2 permeability of AQP1. To assess the influence of the LPR on AQP0 permeability results, we prepared vesicles using molar LPRs of 89 (LPR of 2; mg/mg) for PC/PS/Chl and 500 (LPR of 11.2; mg/mg) for PC/PS/Chl (Figs. S4–S6; Table S2).

The PS/PC/Chl vesicles had a water permeability of 8.25 ± 3.2 μm/s at pH 6.5 and 5.4 ± 1.3 μm/s at pH 7.5 (Fig. 2). These results confirmed that this lipid mixture reduced the water permeability of the vesicles by a factor of ~2 for pH 6.5 compared with pure DMPC, DOPE,

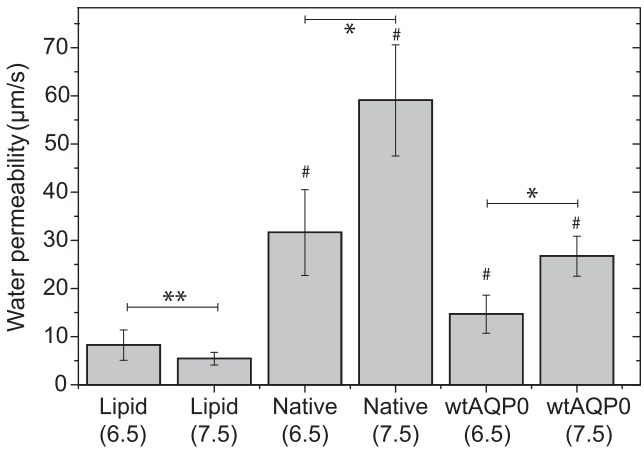

FIGURE 2 Water permeability of AQP0 at pH 6.5 and 7.5. Incorporation of AQP0 purified from sheep lenses (native) and recombinant protein expressed in *P. pastoris* (wtAQP0) results in a significant permeability increase of Chl-rich liposomes ($p < 0.05$ by comparison of proteoliposomes with pure lipid vesicles at each pH using two-way analysis of variance). This result indicates that both native AQP0 and recombinant wtAQPO are functional. The difference in water permeability of native AQP0 and recombinant wtAQP0 at pH 6.5 and 7.5 is small but statistically significant ($p < 0.05$). By comparison, the difference in water permeability of pure lipid vesicles at pH 6.5 and 7.5 is statistically not significant ($p = 0.1$). The error bars represent the standard deviation of the measurements. *$p < 0.05$, **$p = 0.1$, #$p < 0.05$ when compared with pure lipid vesicles. (The p-value is a measure of the probability that the permeability values of vesicles measured under two different conditions will be identical.)

PC/PG and EPL vesicles, and that the water permeability of these vesicles was not significantly different at pH 6.5 and 7.5 (Fig. 2). The effects of forming vesicles in buffers of different pH or dialyzing a vesicle suspension against buffers of different pH were also evaluated, and it was found that these factors did not affect the measured water permeability (data not shown).

Reconstitution of native AQP0 isolated from sheep lenses into the PS/PC/Chl vesicles at an LPR of 2 (mg/mg) resulted in a clearly detectable increase in the water permeability of the proteoliposomes. The water permeability was 31.6 ± 8.9 μm/s at pH 6.5 (an increase by a factor of 3.8 ± 1.8 over control vesicles) and 59.1 ± 11.6 μm/s at pH 7.5 (an increase by a factor of 10.9 ± 3.3; Fig. 2). To ascertain that recombinant sheep AQP0 expressed in *P. pastoris* behaves in the same way as AQP0 directly purified from sheep lenses, we also reconstituted recombinant wtAQP0 into PS/PC/Chl vesicles at an LPR of 2 (mg/mg). The water permeability of the vesicles containing recombinant wtAQP0 was 14.7 ± 4.0 μm/s at pH 6.5 and 26.7 ± 4.15 μm/s at pH 7.5 (increases by factors of 1.8 ± 0.8 and 4.9 ± 1.4, respectively, compared with control vesicles; Fig. 2). Hence, native AQP0 and recombinant wtAQP0 show the same water permeability trends, although the recombinant protein appears to be only about half as conductive for water as the purified native protein (see below).

Effect of tyrosine mutations on AQP0 water conduction

Tyrosine residues 23 and 149 have previously been proposed to be responsible for the low water permeability of AQP0 (9,12,14,15). To experimentally test whether these two tyrosine residues are indeed the cause of the low water permeability of AQP0, we substituted them with the corresponding residues in AQP1, a water channel with a 40-fold higher water permeability than AQP0 (8).

The water permeability of proteoliposomes containing the Y149T mutant was 31.9 ± 10.3 μm/s at pH 6.5, showing that this substitution doubled the water permeability of wtAQP0 (Fig. 3 *A*). The Y23F substitution had a more dramatic effect, increasing the water permeability of proteoliposomes containing this mutant by a factor of ~20 to 294 ± 23.2 μm/s at pH 6.5 (Fig. 3 *A*). Finally, the water permeability of proteoliposomes containing the Y23F/Y149T double mutant was 570 ± 120 μm/s at pH 6.5, a 39-fold increase compared with wtAQP0 (Fig. 3 *A*), demonstrating that the effects of the two tyrosine residues on water permeability are additive.

MD simulations of the water permeability of wtAQP0 and the tyrosine mutants

We performed MD simulations of wtAQP0 and the tyrosine mutants, and used the results to calculate their water permeability values. To mimic a neutral pH, His-40 and His-66 were modeled as singly protonated. From the simulations, we calculated a water permeability of 0.22 × 10^{-14} cm^3/s for the wild-type protein (Fig. 3 *B*), which is similar to the experimentally determined water permeability of ~0.20 × 10^{-14} cm^3/s (estimated assuming 100% incorporation of protein into liposomes from an experimental proteoliposome permeability measurement of 31.6 ± 8.9 μm/s; Fig. 2). Mutation of Tyr-23 to phenylalanine increased the water permeability to 2.9 ± 0.2 × 10^{-14} cm^3/s, a 13-fold increase compared with that of the wild-type protein. Mutation of Tyr-149 to threonine had a lesser effect and increased the water permeability only to 1.0 ± 0.3 × 10^{-14} cm^3/s, a 4.6-fold increase compared with that of the wild-type protein. With a value of 2.5 ± 0.3 × 10^{-14} cm^3/s, the water permeability of the double mutant Y23F/Y149T is similar to that of the single Y23F mutant. A possible explanation for why the effects of the two tyrosine mutations are not additive, as seen in the stopped-flow measurements, is that the introduction of the two mutations causes a large

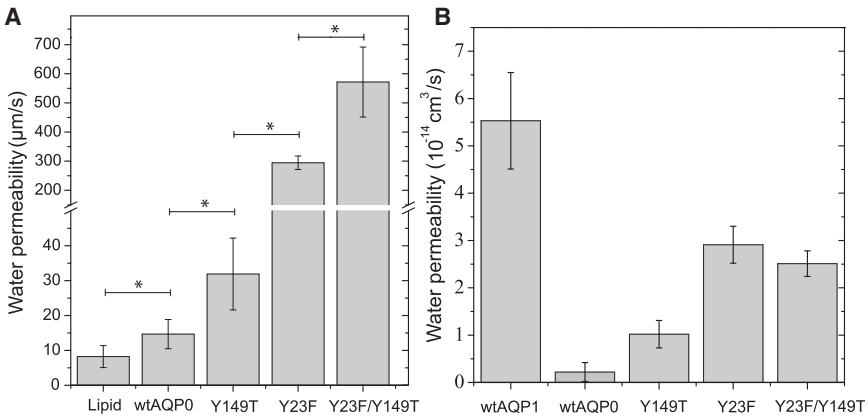

FIGURE 3 (*A*) Water permeability at pH 6.5 of wtAQP0 and mutants in which tyrosine residues were mutated to the corresponding residues in AQP1. Mutation of Tyr-149 to threonine increases the water permeability by a factor of ~2 over wtAQP0. Mutation of Tyr-23 to phenylalanine increases the water permeability by a factor of ~20. The water permeability of the Y23F/Y149T double mutant is ~40 times higher than that of wtAQP0, showing that the effects of the two tyrosine residues are additive. The error bars represent the standard deviation of the measurements; $*p < 0.05$. (*B*) Water permeability of wtAQP0 and mutant AQP0 calculated from MD simulations. The water permeability values calculated from the MD simulations qualitatively agree with those obtained from stopped-flow measurements, with both tyrosine mutations in AQP0, Y149T and Y23F, increasing the water permeability. However, in the MD simulations, the effects of the two tyrosine mutations are not additive. The error bars are standard deviations over the four monomers in the AQP tetramers.

conformational change that cannot relax to an equilibrium ensemble within the submicrosecond timescale of the MD simulation. As the Y23F mutation showed a stronger effect on water permeability in the simulations, we focused on understanding the mechanism by which this mutation increased the water permeability.

We first tested the hypothesis that the increased permeability of the Y23F mutant could be due to a passive widening of the channel pore. For this purpose, we compared the equilibrium radius profile of the wild-type protein with those of the tyrosine mutants. We did find an increase in the average channel radius for the Y23F mutant in the Tyr-23 region (Fig. 4). Similarly, the Y149T mutation caused a widening of the pore in the Tyr-149 regions, and both increases in pore diameter were found in the Y23F/Y149T double mutant (Fig. 4). However, the observed changes are within the standard deviations of the radii computed from the simulations. Thus, a purely static structural change in AQP0 likely does not explain the experimentally measured change in AQP0 water permeability due to the tyrosine mutations.

FMA

Next, we investigated whether a dynamic component could be involved in the modulation of AQP0 water permeability. To this end, we employed PLS-FMA, an approach based on machine learning (30,31). Using this algorithm (see Materials and Methods for details), we identified three distinct functional modes that best correlated with the observed changes in the radius profile of the channel pore (Figs. 5 and S7). These modes, which were calculated in an unbiased manner, identified the residues that are most affected by the introduced mutations. In the region spanning -8 to 0 Å (Fig. 5), motions of Arg-187 make the greatest contribution to changes in the channel radius. In this arginine gate mode, Arg-187 undergoes a gate-like retraction motion that enlarges the pore in its open state or completely occludes the pore in its closed state. In the 0–8 Å region, the largest effect on the channel radius comes from motions of Tyr-23, and is thus termed the Tyr-23 mode. Finally, in the 8–16 Å region, motions of Tyr-149 affect the channel radius the most; thus, this is named the Tyr-149 mode. These results show that the tyrosine mutations target the residues that are responsible for the modulation of the channel radius. Interestingly, the predictive power, measured as the cross-validation correlation coefficient of a mode, decreases in the region in which the mutation is introduced (Fig. S7). This finding indicates that residues Tyr-23 and Tyr-149 modulate the radius profile of the channel in their vicinity and that this effect is reduced upon mutation.

ED simulations

The PLS-FMA methodology establishes a correlation between the radius profile of the channel and the dynamics of the protein, but the characteristic of interest for the channel is its water permeability. To test for a correlation as well as a possible causal relationship between the PLS-FMA modes and water permeability, the ED methodology was used to lock the protein in either the open or closed end state of the PLS-FMA modes. The water permeability values were then calculated for proteins restrained in these two extreme states for each of the three modes (Fig. 6). The water permeability of wtAQP0 only increased to the level observed for the Y23F mutant in the open state of the arginine gate. The open states of the other two modes also increased the water permeability of AQP0, but only marginally. Interestingly, when all three modes were held

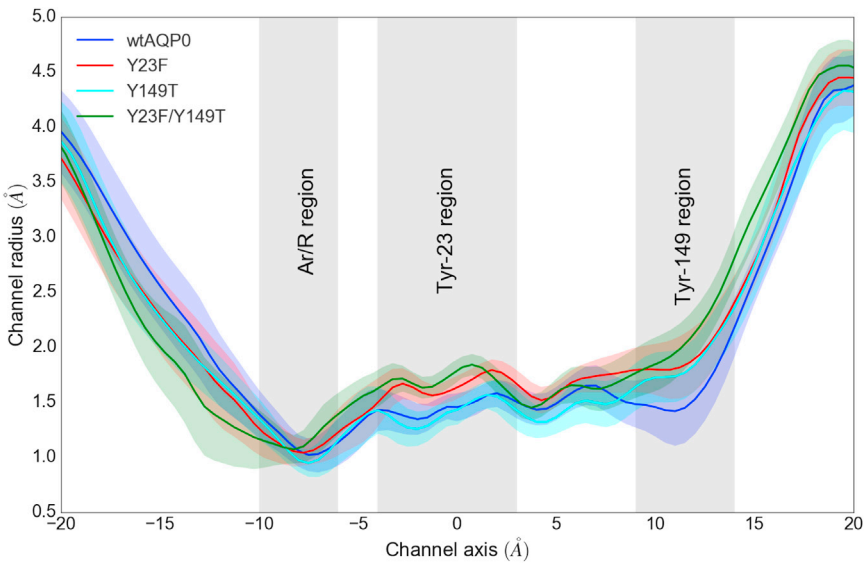

FIGURE 4 Radius profiles of wtAQP0 and the tyrosine mutants. The shaded regions around each profile represent the standard deviation of the channel radii along the simulation trajectories. To see this figure in color, go online.

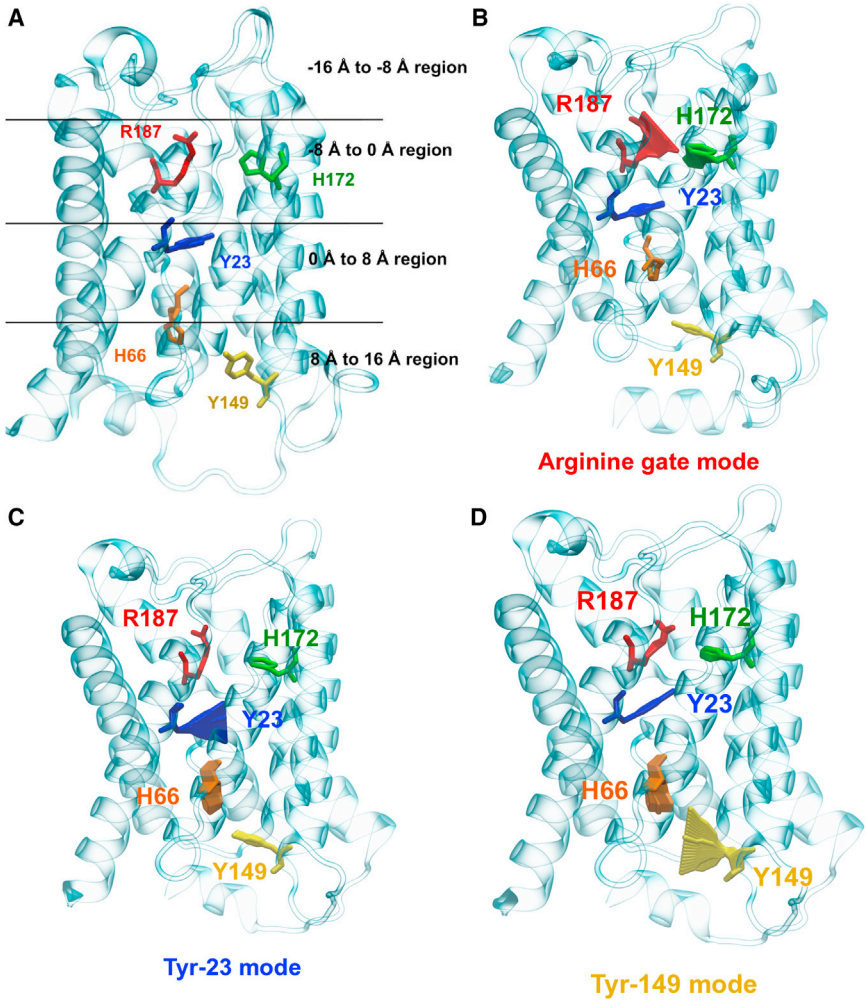

FIGURE 5 Collective modes predicted by partial least-squares-based functional mode analysis (PLS-FMA). (*A*) For FMA, the monomer was divided into four equal, 8 Å long regions along the channel axis. Residues identified to be important for stabilizing the open state of the channel are shown in stick representation. We identified three distinct modes from each region used for FMA analysis that mostly correlate with the change in pore radius. Their motion indicates the contribution of the labeled residues. (*B*) In the arginine gate mode, it is mostly residue Arg-187 that contributes to the mode. (*C* and *D*) The second and third modes are termed the Tyr-23 (*C*) and Tyr-149 (*D*) modes, according to the tyrosine residues that mostly contribute to these modes. To see this figure in color, go online.

in the closed state, the water permeability of the Y23F mutant dropped to that of wtAQP0 (Fig. 6).

Mutations that stabilize the arginine gate of AQP0 in the open state

The results from the ED simulations suggested that mutations that retract Arg-187 and thus hold the arginine gate in the open state should increase the water permeability of AQP0. Seven residues in close proximity to Arg-187 were chosen for further investigation (Fig. S8). Except for Leu-28 and Pro-191, the majority of these residues (Leu-116, Ala-117, Leu-118, Asn-119, and Thr-120) are located in extracellular loop C of AQP0. These residues were systematically mutated in silico to a negatively charged residue, glutamate or aspartate, in an attempt to stabilize the positively charged Arg-187 residue in the open state of the arginine gate (Fig. S8). The water permeability of the 14 mutants could not be calculated from the simulations, as the values did not converge within the simulation window of 300 ns. However, in these unrestrained simulations, the arginine gate of all 14 mutants remained in the open state, which was ascertained by projecting the simulation trajectories for the 14 mutations on the arginine gate mode and comparing their population distributions with that of the native protein (Fig. S9). This result indicates that a residue creating an electrostatic attraction for Arg-187 may indeed stabilize the arginine gate in an open state.

To validate this hypothesis, all 14 mutants were targeted experimentally. Although most of the proteins carrying these mutations could not be expressed, the T120E mutant could be purified and showed increased water permeability (Fig. S10), indicating that the predicted mechanism captures the structural cause behind the modulation of AQP0 water permeability.

pH sensitivity of AQP0 water conduction

Most studies on the pH sensitivity of AQP0 have been performed with AQP0 expressed in oocytes, raising the possibility that the measured water conduction may have been affected by effects introduced by the oocyte. The water permeability of PS/PC/Chl vesicles is not pH dependent

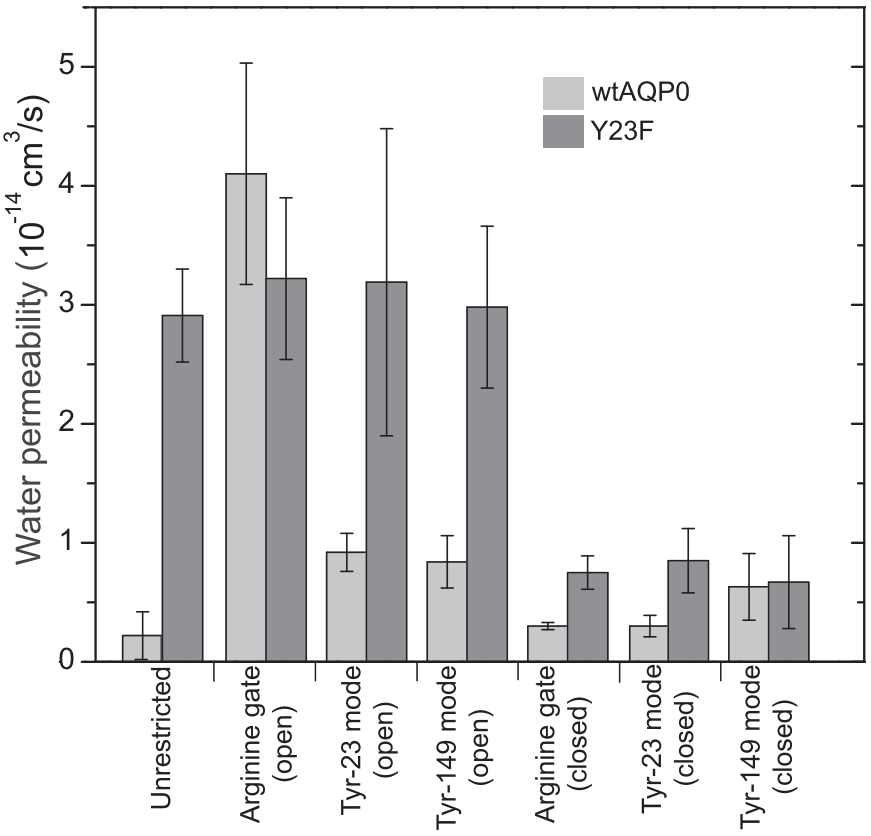

FIGURE 6 Water permeability obtained from essential dynamics (ED) simulations. The water permeabilities of wtAQP0 and the Y23F mutant in the open and closed states of the three modes identified by PLS-FMA are compared.

(8.25 ± 3.2 μm/s at pH 6.5 and 5.4 ± 1.3 μm/s at pH 7.5; Fig. 2), but incorporation of wtAQP0 showed a water permeability of 14.7 ± 4.0 μm/s at pH 6.5 and a permeability of 26.7 ± 4.15 μm/s at pH 7.5, an increase by a factor of 1.9 ± 0.6 (Fig. 2). Similarly, the water conductance of the Y23F mutant at pH 7.5 was 390 ± 50 μm/s, an increase by a factor of 1.3 ± 0.2 compared with its permeability at pH 6.5 (295 ± 23 μm/s; Fig. S11). Two histidine residues in AQP0, His-40 and His-66, have previously been implicated in potentially being responsible for pH sensitivity of AQP0-mediated water conduction (13,16,17). To experimentally test the contribution of these two histidine residues to pH sensitivity, we performed water permeability measurements on AQP0 in which the histidines were substituted. However, given that the water permeability of wtAQP0 is close to that of lipid membranes, even when the proteoliposomes are prepared at an LPR of 2, we introduced the histidine substitutions into the Y23F mutant of AQP0, which has a 20-fold higher water permeability than the wild-type protein. The water permeability of the H40Q/Y23F mutant was 206.5 ± 30.4 μm/s at pH 6.5 and 281 ± 72 μm/s at pH 7.5, an increase by a factor of 1.4 ± 0.4 (Fig. S12). The water permeability of the H66M/Y23F mutant was 218.5 ± 85 μm/s at pH 6.5 and 262 ± 103 μm/s at pH 7.5, an increase by a factor of 1.2 ± 0.7 (Fig. S12). A statistical assessment by analysis of variance shows that the permeability difference between pH 6.5 and 7.5 for both H40Q/Y23F and H66M/Y23F is not significantly different. Hence, mutation of His-40 and His-66 appears to further decrease the already low pH sensitivity of AQP0.

DISCUSSION

Accurate experimental measurement of the water permeation rate of AQP0

Investigators have previously measured the water conduction of AQP0 either by injecting AQP0 cRNA into *Xenopus* oocytes or by reconstituting purified AQP0 protein into lipid vesicles. However, the low permeability of AQP0, which is only slightly higher than that of pure lipid membranes, makes it difficult to measure its water conduction accurately. In the case of oocyte expression, this problem can be alleviated by injecting a high amount of cRNA (8), and indeed all studies that used expression of AQP0 in oocytes showed an observable increase in water permeability over noninjected oocytes (8,16,17,38–41). In contrast, in an early water conduction study using purified AQP0 reconstituted into proteoliposomes, the chosen LPR of 15.3 (mg/mg) resulted in a very small increase in the water permeability of the vesicles by a factor of only 1.2, and therefore AQP0 was not recognized as a water channel (42). In a recent

study, using AQP0 proteoliposomes reconstituted at LPRs ranging from 5.3 to 50 (mg/mg; corresponding to a molar LPR of ~200–1500), permeability measurements were improved by adding Chl to the lipid mixture, which reduced the water leakage of the membrane itself (36). The reported permeability values of AQP0 in that study were still very close to the permeability of the pure lipid vesicles over at least half of the LPRs tested, limiting the accuracy of the measured values. Here, by further lowering the LPR to 2, we were able to improve the accuracy of water permeability measurements for AQP0 (Figs. S4–S6).

A low LPR of 2 ensures a large contribution of the channel to the water permeability of the proteoliposomes. We also optimized the lipid composition of the vesicles to minimize the background permeability of the lipid bilayer by adding Chl at a concentration of 50% (mol/mol). With these optimized AQP0 proteoliposomes, stopped-flow light-scattering spectrometry showed a clear increase in the water permeability of liposomes by a factor of ~11 at pH 7.5 upon incorporation of AQP0 (Fig. 2).

Our measurements were sufficiently accurate to reveal that native AQP0 purified from the lens had a higher water permeability than the recombinant wild-type protein (Fig. 2). Although the difference is small, this result indicates that the water permeability of AQP0 may be affected by posttranslational modifications that are present in the native protein, but not in the recombinant protein. Although we cannot comment on the mechanism through which posttranslational modifications would affect the water permeability of AQP0, it is unlikely to involve the arginine gate mechanism. Nevertheless, our measurements suggest that vesicles that are made with Chl and contain a high concentration of AQP0 make it possible to measure AQP0-mediated water conduction accurately (see Figs. S5 and S6). Still, even proteoliposomes containing native AQP0 have a very low water permeability of 31.6 $\pm$ 8.9 μm/s, which is only slightly higher than the permeability of pure lipid bilayers. However, lens membranes are highly enriched in Chl, with a molar ratio of Chl to phospholipid of ~5:1 in human lens membranes (43–45), substantially reducing the water permeability of these membranes. Therefore, even with its low water conduction rate, AQP0 will markedly increase the water permeability of lens membranes, particularly considering the high abundance of AQP0 in lens membranes. Interestingly, the water permeability of Killifish AQP0 is an order of magnitude higher than that of bovine AQP0 (17). This observation led to the proposal that low water permeability may have been a mammalian evolutionary adaption of AQP0 to dry-air environments (10).

Effect of Tyr-23 and Tyr-149 on the water permeability of AQP0

Even though AQP0 has the typical AQP fold, its water conductance is the lowest among all AQPs (38). It was proposed that the low water permeability of AQP0 would help maintain lens structure by ensuring a uniform cell response to osmotic imbalances (12). In addition to its function as a water channel, AQP0 mediates cell-cell junctions between fiber cells, thus helping to minimize gaps between neighboring fiber cells, which is necessary for the lens to remain transparent (3). Another reason that was proposed for the low water permeability of AQP0 was thus to not compromise the stability of AQP0-mediated cell-cell junctions (9).

By comparing the atomic structure of AQP0 with that of AQP1, which is 40 times more permeable for water than AQP0 (8), one can see that many residues that line the channel in AQP0 are larger and more hydrophobic than those found in AQP1, resulting in a narrower, longer pore with an additional constriction site close to the cytoplasmic entrance of the pore known as constriction site II (CS II) (13). Previous MD simulations reported that in silico mutation of Tyr-23 to phenylalanine increases the water permeation rate of AQP0 by a factor of 2–4 (15). Thus, Tyr-23 alone could not explain the 40-fold lower water permeation rate of AQP0 compared with AQP1. Our experimental measurements show, however, that the Y23F mutation increases the water conduction of AQP0 by a factor of 20 (much more than predicted by the previous MD simulation study), establishing that the hydroxyl group of the Tyr-23 side chain is in fact the major reason for the low water permeability of AQP0.

Other MD simulations have also hinted that Tyr-149 in CS II of AQP0 serves as another factor in the slow water conduction, though to a lesser extent than Tyr-23 (9). Under conditions of 1.8 mM Ca^{2+}, the permeability of AQP0 is known to decrease by a factor of 2 due to the allosteric binding of calmodulin, which introduces a mechanical strain at CS II (46). Mutation of Phe-149 to glycine eliminated the sensitivity of AQP0 water conductance to Ca^{2+}-calmodulin when expressed in oocytes, and effectively increased AQP0 water permeability by a factor of 2 in the presence of 1.8 mM Ca^{2+} (46). Our measurements of AQP0 proteoliposomes confirm that the Y149T mutation increases the water permeability of AQP0 twofold. Furthermore, in our stopped-flow measurements (albeit not in our MD simulations), the effects of the two tyrosine mutations, Y23F and Y149T, are additive. As a result, the water permeability of the Y23F/Y149T double mutant is ~40-fold higher than that of the wild-type protein. This result indicates that the difference in water permeability between AQP1 and AQP0 is almost exclusively due to the combined effects of the two tyrosine residues extending into the AQP0 water pathway.

Mechanism of the water permeability modulation

The MD simulations helped to shed light on the mechanism by which channel-lining residues modulate the water permeability of AQP0. One of the residues involved, Arg-187, is

highly conserved and part of the ar/R region found in all AQP channels. Many previous studies of AQPs have shown that this pore-lining arginine can affect the permeability and selectivity of the AQP channel. For example, the high electrostatic repulsion between protons and Arg-226 and His-212 of the selectivity filter in Aqy1 from *P. pastoris* prevents proton conduction through the pore (47). In AtTIP1 from *Arabidopsis thaliana*, ammonia selectivity is introduced by a unique conformation of Arg-200 that is induced by the presence of a histidine residue in loop C forming an extended selectivity filter (48). Beitz et al. (49) showed by mutagenesis and Newby et al. (50) later confirmed by structural studies that in PfAQP from *Plasmodium falciparum*, Arg-196 is stabilized by Glu-125 in loop C to allow for high water permeability. In AqpZ from *E. coli*, the arginine residue in the constriction region has been crystallographically characterized in two different conformations (51), which in MD simulations correlated with an open and a closed channel state (52).

In the case of AQP0, the three PLS-FMA modes observed in our equilibrium simulations demonstrate that there are collective motions involving multiple residues in the protein that can dynamically change the radius profile of the channel pore. These changes can in turn affect the permeability of the protein, as established by the ED simulations. Although our results show a connection between the PLS-FMA modes and the water permeability of AQP0, the structural basis for how the modes affect water conduction remains unclear. It is also not obvious why opening of the arginine gate alone can increase the water permeability of AQP0 to that of the Y23F mutant, but exert no direct effect on Tyr-23. To address these questions, we considered the population distributions of wtAQP0 and the Y23F mutant along the arginine gate mode (Fig. S13). The distributions showed that the Y23F mutant spends twice as much time in the open state of the arginine gate mode as the wild-type protein. To understand the cause of the change in population distribution as a result of the Y23F mutation, we first looked for any physical connection, such as a hydrogen bond, between residues Arg-187 and Tyr-23, or for any indirect hydrogen-bond network between the two residues through another residue that would be disrupted due to the mutation. However, we observed no such interactions in the simulations. A potential explanation emerged when we studied the water densities within the channel pore in the ED simulations. When the arginine gate is held in the open state, the water densities for both wtAQP0 (Fig. 7 *A*) and the Y23F mutant (Fig. 7 *C*) appear identical. However, when the arginine gate is held in the closed configuration, Tyr-23 in wtAQP0 can trap a single water molecule (visible in its density profile) between Arg-187 and Tyr-23, creating a water-based, hydrogen-bonding bridge (Fig. 7 *B*). This bridge may explain how the Y23F mutation, which results in the loss of the hydroxyl group of Tyr-23, can no longer

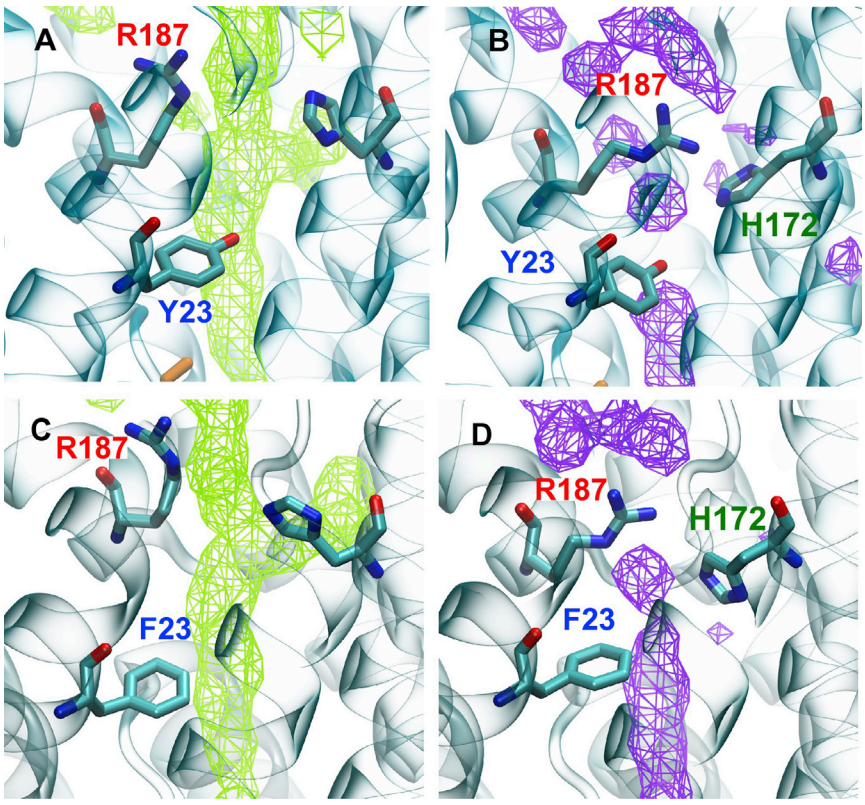

FIGURE 7 Water density in the AQP0 channel lumen as observed in the ED simulations. (*A* and *B*) Water density in the open (*A*) and closed (*B*) states of wtAQP0 in the arginine gate mode. (*C* and *D*) Water density in the open (*C*) and closed (*D*) states of the Y23F mutant in the arginine gate mode. A water molecule between residues Arg-187 and Tyr-23 stabilizes the closed state for the wild-type protein (*B*), but not for the Y23F mutant (*D*). To see this figure in color, go online.

maintain a similar bridging hydrogen-bonding interaction (Fig. 7 *D*). Thus, water in the region between residue 23 and Arg-187 is more mobile in the Y23F mutant than in the wild-type protein. This interaction points to the structural mechanism by which the mutant increases the water permeability of AQP0. Tyr-23 appears to modulate the arginine gate by holding the Arg-187 residue in the closed configuration due to the bridged hydrogen bond, whereas in the Y23F mutant Arg-187 is more likely to remain in the open configuration.

The ar/R region is the narrowest region in AQP channels (Fig. 4), and changes that greatly increase water permeability must widen the channel pore in this region. The low water permeability of AQP0 is due to a bridging water molecule that holds Arg-187 of the ar/R region in the closed state of the arginine gate. This explains why the Tyr-23 and Tyr-149 modes in wtAQP0 can switch the protein to a low permeability state but cannot increase the permeability to the same level as the Y23F mutation. The Tyr-23 mode in its closed state acts by restricting the water molecule between Tyr-23 and Arg-187 even further, thus favoring the closed state of the arginine gate. The Tyr-149 mode can act as a gate that can constrict the pore at the cytoplasmic side of the protein. In their open states, however, neither mode can effectively alter the channel profile at the narrowest region of the protein, the arginine gate. Thus, the arginine gate mode will always dominate the permeation behavior. As the Tyr-149 mode and the arginine gate mode can act independently of each other, their effects on the water permeability of AQP0 can be additive.

Corroborating the role of the arginine gate mode, we find that mutations predicted to keep the channel pore open show a strong effect on the population distributions of the protein along the arginine gate mode. All of these mutations tend to favor the open state of the mode. However, in the simulations of these mutations, we could not calculate the permeability due to a lack of convergence. The reason for this could be structural changes in the protein due to the introduction of a negative charge in the conserved ar/R region that do not equilibrate on the submicrosecond timescale of the simulations.

pH sensitivity of AQP0 water conduction

The pH of the eye lens ranges from 6.81 at a radius of 30% of the total radius of the lens to 7.02 at a fractional radius of 90% (53). It is therefore of interest to establish whether the water permeability of AQP0 is affected by pH. Although some studies did not detect any changes in AQP0 water conduction under different pH conditions (19,20), other studies found that the water permeability of AQP0 at pH 6.5 was two- to fourfold higher than that under lower or higher pH conditions (16–18). Although the water conduction does not change greatly under different pH conditions, considering the high abundance of AQP0 in lens fiber membranes, even a small difference may still be physiologically relevant.

We found that native AQP0 and the recombinant wild-type protein have a slightly higher water permeability at pH 7.5 than at pH 6.5 (Fig. 2). We observed the same pH behavior for the Y23F, Y149T, and Y23F/Y149T mutants (Fig. S12). Although the effect is small and decreases further with mutation of H40 and H66 in the Y23F mutant (Fig. S12), it is not only consistent for all analyzed AQP0 variants but is also statistically significant as assessed by Student's *t*-test. We therefore conclude that water conduction by AQP0 is pH sensitive and that it is higher by a factor of ~1.5 at pH 7.5. With regard to other pore-lining histidine residues, AQP1 has a histidine, His-182, that corresponds to His-172 in AQP0 (Fig. S14) (16). Since both water channels have this histidine, but only AQP0 (and not AQP1) is pH sensitive, this residue is unlikely to play a role in pH sensing. Furthermore, Arg-187 of AQP0 and Arg-197 of AQP1 are in close proximity to His-172 and His-182, respectively. The proximity of the arginine residues to the histidine residues likely shifts the pKa of the histidine residues beyond the physiological range. The pH behavior we measured with AQP0 reconstituted into proteoliposomes is the opposite of what has previously been reported for AQP0 expressed in oocytes (13,16,17). Although this is surprising, a similar observation was reported for Ca^{2+} regulation of AQP0: Ca^{2+} caused a fourfold decrease in the permeability of AQP0 expressed in oocytes, but resulted in a 2.5-fold increase in the permeability of proteoliposomes formed from native lens membranes (18,54). These results suggest that the biological environment AQP0 encounters in a *Xenopus* oocyte modifies its permeability and regulation.

SUPPORTING MATERIAL

Fourteen figures and two tables are available at http://www.biophysj.org/biophysj/supplemental/S0006-3495(17)30148-0.

AUTHOR CONTRIBUTIONS

Designed research: M.K., T.W., B.L.d.G., C.R., P.O.S., and S.K. Performed research: P.O.S., C.R., S.K., Y.-S.H., S.R.S., R.D.Z., and J.Y. Analyzed data: M.K., P.O.S., S.K., B.L.d.G., and T.W. Wrote the manuscript: P.O.S., M.K., B.L.d.G., and T.W.

ACKNOWLEDGMENTS

We thank Dr. Timothy Springer and Dr. Kyle Bishop for providing access to light-scattering equipment, and the Shared Fermentation Facility of Penn State for providing access to bioprocessing equipment.

Work on AQP0 in the Walz laboratory was supported by National Institutes of Health grant R01 EY015107. B.L.d.G. received funding from the German Research Foundation via SFB803 (Project A03). P.O.S. received funding from the United States Environmental Protection Agency under the Science to Achieve Results (STAR) Graduate Fellowship Program.

This work was supported in part by National Science Foundation grant CBET- 1512099 to M.K.

REFERENCES

1. Gerometta, R., A. C. Zamudio, …, O. A. Candia. 2007. Volume change of the ocular lens during accommodation. *Am. J. Physiol. Cell Physiol.* 293:C797–C804.
2. Alcalá, J., N. Lieska, and H. Maisel. 1975. Protein composition of bovine lens cortical fiber cell membranes. *Exp. Eye Res.* 21:581–595.
3. Costello, M. J., T. J. McIntosh, and J. D. Robertson. 1989. Distribution of gap junctions and square array junctions in the mammalian lens. *Invest. Ophthalmol. Vis. Sci.* 30:975–989.
4. Donaldson, P., J. Kistler, and R. T. Mathias. 2001. Molecular solutions to mammalian lens transparency. *News Physiol. Sci.* 16:118–123.
5. Mathias, R. T., J. L. Rae, and G. J. Baldo. 1997. Physiological properties of the normal lens. *Physiol. Rev.* 77:21–50.
6. Zampighi, G., S. A. Simon, …, M. J. Costello. 1982. On the structural organization of isolated bovine lens fiber junctions. *J. Cell Biol.* 93:175–189.
7. Chepelinsky, A. B. 2009. Structural function of MIP/aquaporin 0 in the eye lens; genetic defects lead to congenital inherited cataracts. *Handb. Exp. Pharmacol.* 190:265–297.
8. Chandy, G., G. A. Zampighi, …, J. E. Hall. 1997. Comparison of the water transporting properties of MIP and AQP1. *J. Membr. Biol.* 159:29–39.
9. Jensen, M. O., R. O. Dror, …, D. E. Shaw. 2008. Dynamic control of slow water transport by aquaporin 0: implications for hydration and junction stability in the eye lens. *Proc. Natl. Acad. Sci. USA.* 105:14430–14435.
10. Calvanese, L., M. Pellegrini-Calace, and R. Oliva. 2010. Mutations at key pore-lining positions differentiate the water permeability of fish lens aquaporin from other vertebrates. *FEBS Lett.* 584:4797–4801.
11. Gonen, T., Y. Cheng, …, T. Walz. 2005. Lipid-protein interactions in double-layered two-dimensional AQP0 crystals. *Nature.* 438:633–638.
12. Harries, W. E. C., D. Akhavan, …, R. M. Stroud. 2004. The channel architecture of aquaporin 0 at a 2.2-A resolution. *Proc. Natl. Acad. Sci. USA.* 101:14045–14050.
13. Gonen, T., P. Sliz, …, T. Walz. 2004. Aquaporin-0 membrane junctions reveal the structure of a closed water pore. *Nature.* 429:193–197.
14. Hashido, M., M. Ikeguchi, and A. Kidera. 2005. Comparative simulations of aquaporin family: AQP1, AQPZ, AQP0 and GlpF. *FEBS Lett.* 579:5549–5552.
15. Qiu, H., S. Ma, …, W. Guo. 2010. Dynamic and energetic mechanisms for the distinct permeation rate in AQP1 and AQP0. *Biochim. Biophys. Acta.* 1798:318–326.
16. Németh-Cahalan, K. L., and J. E. Hall. 2000. pH and calcium regulate the water permeability of aquaporin 0. *J. Biol. Chem.* 275:6777–6782.
17. Németh-Cahalan, K. L., K. Kalman, and J. E. Hall. 2004. Molecular basis of pH and Ca^{2+} regulation of aquaporin water permeability. *J. Gen. Physiol.* 123:573–580.
18. Varadaraj, K., S. Kumari, …, R. T. Mathias. 2005. Regulation of aquaporin water permeability in the lens. *Invest. Ophthalmol. Vis. Sci.* 46:1393–1402.
19. Virkki, L. V., G. J. Cooper, and W. F. Boron. 2001. Cloning and functional expression of an MIP (AQP0) homolog from killifish (Fundulus heteroclitus) lens. *Am. J. Physiol. Regul. Integr. Comp. Physiol.* 281:R1994–R2003.
20. Zeuthen, T., and D. A. Klaerke. 1999. Transport of water and glycerol in aquaporin 3 is gated by H(+). *J. Biol. Chem.* 274:21631–21636.
21. Gonen, T., P. Donaldson, and J. Kistler. 2000. Galectin-3 is associated with the plasma membrane of lens fiber cells. *Invest. Ophthalmol. Vis. Sci.* 41:199–203.
22. Cordingley, M. G., R. B. Register, …, R. J. Colonno. 1989. Cleavage of small peptides *in vitro* by human rhinovirus 14 3C protease expressed in *Escherichia coli*. *J. Virol.* 63:5037–5045.
23. Kumar, M., M. Grzelakowski, …, W. Meier. 2007. Highly permeable polymeric membranes based on the incorporation of the functional water channel protein Aquaporin Z. *Proc. Natl. Acad. Sci. USA.* 104:20719–20724.
24. Wang, J. 2008. Electrochemical glucose biosensors. *Chem. Rev.* 108:814–825.
25. Foloppe, N., and A. D. MacKerell, Jr. 2000. All-atom empirical force field for nucleic acids: I. Parameter optimization based on small molecule and condensed phase macromolecular target data. *J. Comput. Chem.* 21:86–104.
26. Darden, T., D. York, and L. Pedersen. 1993. Particle mesh Ewald: an $N\cdot\log(N)$ method for Ewald sums in large systems. *J. Chem. Phys.* 98:10089–10092.
27. Bussi, G., D. Donadio, and M. Parrinello. 2007. Canonical sampling through velocity rescaling. *J. Chem. Phys.* 126:014101.
28. Abraham, M. J., T. Murtola, …, E. Lindahl. 2015. GROMACS: high performance molecular simulations through multi-level parallelism from laptops to supercomputers. *SoftwareX.* 1–2:19–25.
29. Zhu, F., E. Tajkhorshid, and K. Schulten. 2004. Collective diffusion model for water permeation through microscopic channels. *Phys. Rev. Lett.* 93:224501.
30. Krivobokova, T., R. Briones, …, B. L. de Groot. 2012. Partial least-squares functional mode analysis: application to the membrane proteins AQP1, Aqy1, and CLC-ec1. *Biophys. J.* 103:786–796.
31. Hub, J. S., and B. L. de Groot. 2009. Detection of functional modes in protein dynamics. *PLoS Comput. Biol.* 5:e1000480.
32. Kaptan, S., M. Assentoft, …, B. L. de Groot. 2015. H95 is a pH-dependent gate in aquaporin 4. *Structure.* 23:2309–2318.
33. Smart, O. S., J. G. Neduvelil, …, M. S. Sansom. 1996. HOLE: a program for the analysis of the pore dimensions of ion channel structural models. *J. Mol. Graph.* 14:354–360, 376.
34. Amadei, A., A. B. Linssen, and H. J. Berendsen. 1993. Essential dynamics of proteins. *Proteins.* 17:412–425.
35. Mathai, J. C., S. Tristram-Nagle, …, M. L. Zeidel. 2008. Structural determinants of water permeability through the lipid membrane. *J. Gen. Physiol.* 131:69–76.
36. Tong, J., J. T. Canty, …, T. J. McIntosh. 2013. The water permeability of lens aquaporin-0 depends on its lipid bilayer environment. *Exp. Eye Res.* 113:32–40.
37. Itel, F., S. Al-Samir, …, V. Endeward. 2012. CO_2 permeability of cell membranes is regulated by membrane cholesterol and protein gas channels. *FASEB J.* 26:5182–5191.
38. Yang, B., and A. S. Verkman. 1997. Water and glycerol permeabilities of aquaporins 1-5 and MIP determined quantitatively by expression of epitope-tagged constructs in *Xenopus* oocytes. *J. Biol. Chem.* 272:16140–16146.
39. Mulders, S. M., G. M. Preston, …, P. Agre. 1995. Water channel properties of major intrinsic protein of lens. *J. Biol. Chem.* 270:9010–9016.
40. Varadaraj, K., C. Kushmerick, …, R. T. Mathias. 1999. The role of MIP in lens fiber cell membrane transport. *J. Membr. Biol.* 170:191–203.
41. Reichow, S. L., and T. Gonen. 2008. Noncanonical binding of calmodulin to aquaporin-0: implications for channel regulation. *Structure.* 16:1389–1398.
42. Van Hoek, A. N., M. Wiener, …, A. S. Verkman. 1993. Secondary structure analysis of purified functional CHIP28 water channels by CD and FTIR spectroscopy. *Biochemistry.* 32:11847–11856.

43. Deeley, J. M., T. W. Mitchell, …, R. J. Truscott. 2008. Human lens lipids differ markedly from those of commonly used experimental animals. *Biochim. Biophys. Acta.* 1781:288–298.

44. Fleschner, C. R., and R. J. Cenedella. 1991. Lipid composition of lens plasma membrane fractions enriched in fiber junctions. *J. Lipid Res.* 32:45–53.

45. Rujoi, M., J. Jin, …, M. C. Yappert. 2003. Isolation and lipid characterization of cholesterol-enriched fractions in cortical and nuclear human lens fibers. *Invest. Ophthalmol. Vis. Sci.* 44:1634–1642.

46. Reichow, S. L., D. M. Clemens, …, T. Gonen. 2013. Allosteric mechanism of water-channel gating by Ca^{2+}-calmodulin. *Nat. Struct. Mol. Biol.* 20:1085–1092.

47. Kosinska Eriksson, U., G. Fischer, …, R. Neutze. 2013. Subangstrom resolution X-ray structure details aquaporin-water interactions. *Science.* 340:1346–1349.

48. Kirscht, A., S. S. Kaptan, …, U. Johanson. 2016. Crystal structure of an ammonia-permeable aquaporin. *PLoS Biol.* 14:e1002411.

49. Beitz, E., S. Pavlovic-Djuranovic, …, J. E. Schultz. 2004. Molecular dissection of water and glycerol permeability of the aquaglyceroporin from *Plasmodium falciparum* by mutational analysis. *Proc. Natl. Acad. Sci. USA.* 101:1153–1158.

50. Newby, Z. E., J. O'Connell, 3rd, …, R. M. Stroud. 2008. Crystal structure of the aquaglyceroporin PfAQP from the malarial parasite *Plasmodium falciparum*. *Nat. Struct. Mol. Biol.* 15:619–625.

51. Jiang, J., B. V. Daniels, and D. Fu. 2006. Crystal structure of AqpZ tetramer reveals two distinct Arg-189 conformations associated with water permeation through the narrowest constriction of the water-conducting channel. *J. Biol. Chem.* 281:454–460.

52. Xin, L., H. Su, …, Y. Mu. 2011. Water permeation dynamics of AqpZ: a tale of two states. *Biochim. Biophys. Acta.* 1808:1581–1586.

53. Mathias, R. T., G. Riquelme, and J. L. Rae. 1991. Cell to cell communication and pH in the frog lens. *J. Gen. Physiol.* 98:1085–1103.

54. Kalman, K., K. L. Németh-Cahalan, …, J. E. Hall. 2008. Phosphorylation determines the calmodulin-mediated Ca^{2+} response and water permeability of AQP0. *J. Biol. Chem.* 283:21278–21283.

Biophysical Journal, Volume *112*

Supplemental Information

Role of Pore-Lining Residues in Defining the Rate of Water Conduction by Aquaporin-0

Patrick O. Saboe, Chiara Rapisarda, Shreyas Kaptan, Yu-Shan Hsiao, Samantha R. Summers, Rita De Zorzi, Danijela Dukovski, Jiaheng Yu, Bert L. de Groot, Manish Kumar, and Thomas Walz

Supplementary Information

Role of pore-lining residues in defining the rate of water conduction by aquaporin-0

Table S1. Increase in water permeability of AQP0 proteoliposomes prepared with low lipid-to-protein ratios compared to pure lipid vesicles.

Lipid	LPR (mg/mg)	mLPR (mol/mol)	Factor increase in water permeability of AQP0 proteoliposomes over that of control vesicles
DMPC	2.0	78	3.5 ± 0.8
PC/PG 4:1 (mol/mol)	2.6	89	2.2 ± 0.8
E. coli polar lipids	2.4	78	2.2 ± 0.3

Table S2. Increase in water permeability of AQP0 proteoliposomes prepared with different lipid-to-protein ratios compared to pure lipid vesicles and the effect of cholesterol. Addition of cholesterol decreases the water leakage through the lipid bilayers, making it easier to measure the increase in water permeability due to AQP0.

Lipid	LPR (mg/mg)	mLPR (mol/mol)	Factor increase in water permeability of AQP0 proteoliposomes over that of control vesicles
PC/PG 4:1 (mol/mol)	14.9	500	1.3 ± 0.7
	2.6	89	2.2 ± 0.8
PC/PG/Chl 2:1:2 (mol/mol)	11.9	500	2.0 ± 0.5
	2.1	89	3.0 ± 0.9
PC/PS/Chl 4:1:5 (mol/mol)	11.2	500	1.5 ± 0.6
	2.0	89	3.8 ± 1.8

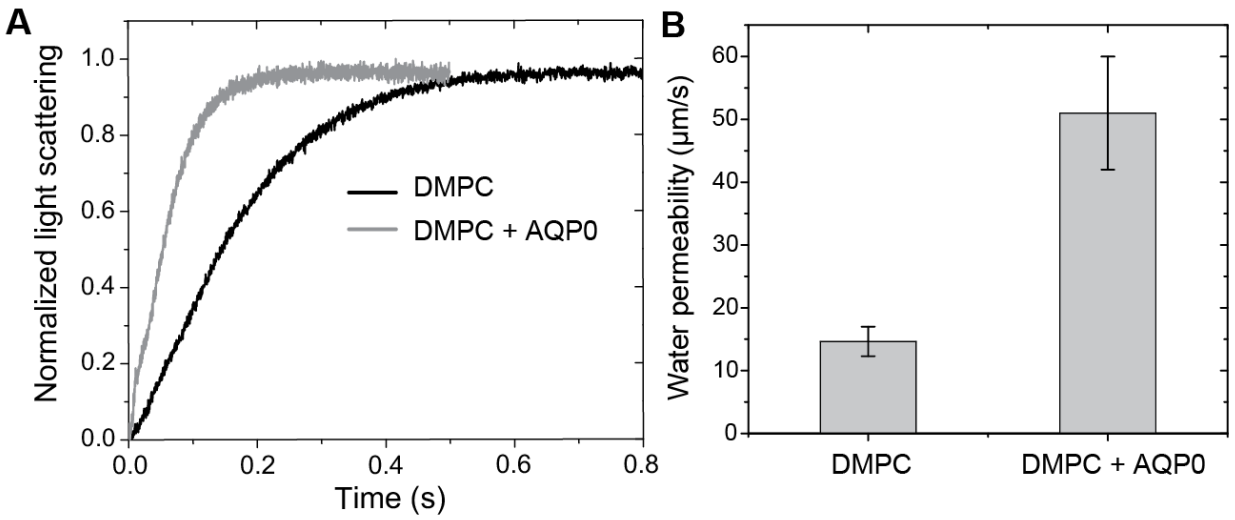

Figure S1. Water permeability of pure DMPC vesicles and AQP0-containing DMPC proteoliposomes. A) Stopped-flow light scattering traces obtained with pure DMPC vesicles (black trace) and AQP0 proteoliposomes resulting from reconstitution at an LPR of 2 (mg/mg; molar LPR of 78) (gray trace). **B)** The water permeability of pure DMPC vesicles at pH 6.5 was 14.7 ± 2.3 µm/s and that of the AQP0 proteoliposomes was 51.0 ± 9.0 µm/s, corresponding to an increase by a factor of 3.5 ± 0.8. The values are the average of three independent measurements and the error bars represent the standard deviation of the measurements. For DMPC, the experimental temperatures were adjusted to stay above the phase transition temperature of the lipid (37ºC was used for dialysis and 25ºC was used for stopped-flow measurements).

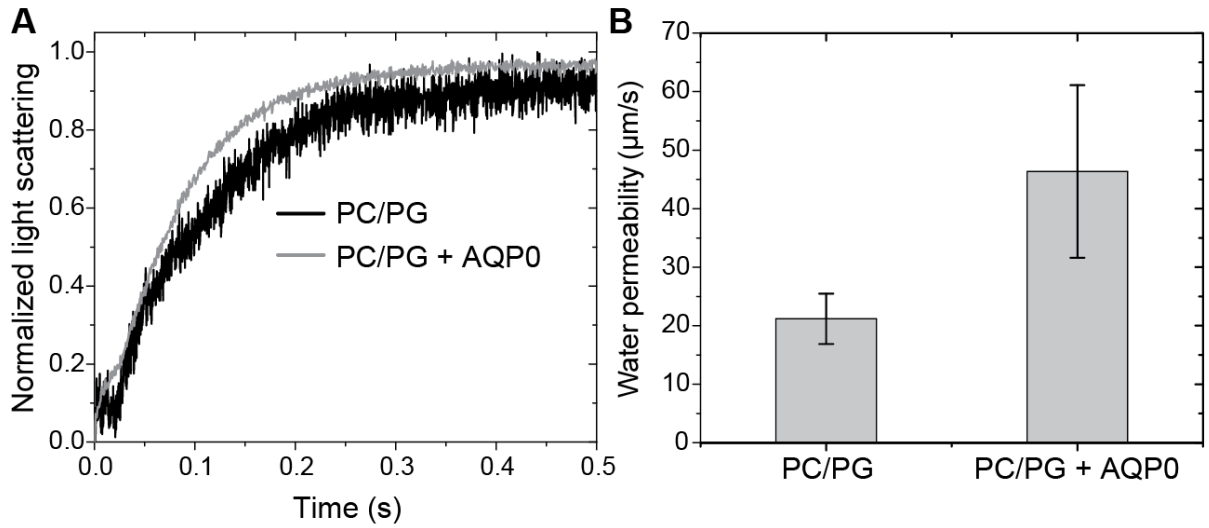

Figure S2. Water permeability of pure PC/PG (molar ratio of 4:1) vesicles and AQP0-containing PC/PG proteoliposomes. A) Stopped-flow light scattering traces obtained with pure PC/PG vesicles (black trace) and AQP0 proteoliposomes resulting from reconstitution at an LPR of 2.6 (mg/mg; molar LPR of 89) (gray trace). **B)** The water permeability of pure PC/PG vesicles at pH 6.5 was 21.2 ± 4.3 µm/s and that of the AQP0 proteoliposomes was 46.4 ± 14.8 µm/s, corresponding to an increase by a factor of 2.2 ± 0.8. The values are the average of three independent measurements and the error bars represent the standard deviation of the measurements.

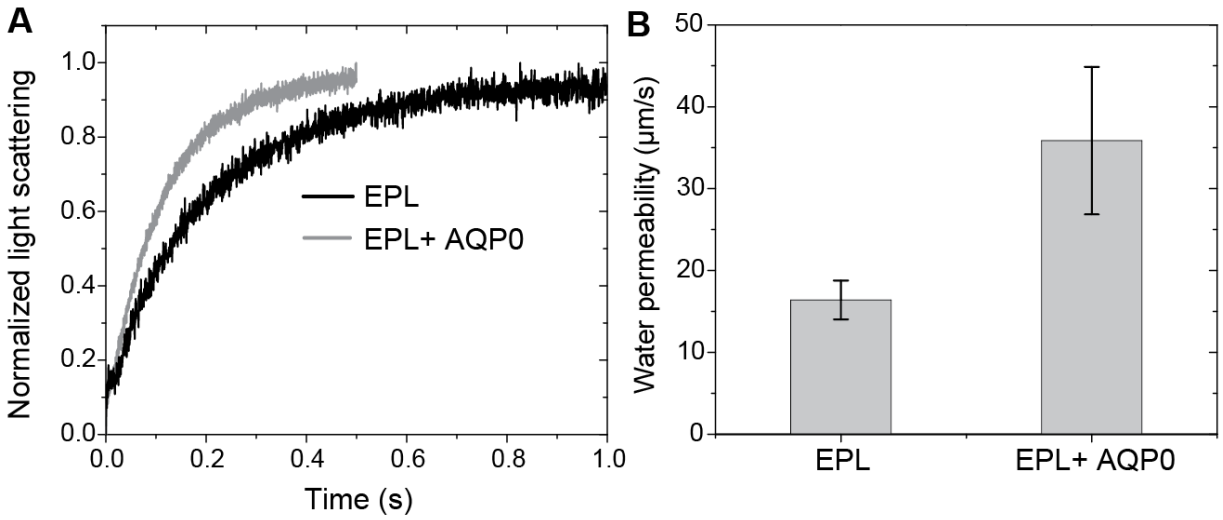

Figure S3. Water permeability of pure *E. coli* polar lipids (EPL) vesicles and AQP0-containing EPL proteoliposomes. A) Stopped-flow light scattering traces obtained with pure EPL vesicles (black trace) and AQP0 proteoliposomes resulting from reconstitution at an LPR of 2.4 (mg/mg; molar LPR of 78) (gray trace). **B)** The water permeability of pure EPL vesicles at pH 6.5 was 16.4 ± 1.4 µm/s and that of the AQP0 proteoliposomes was 35.9 ± 1.0 µm/s, corresponding to an increase by a factor of 2.19 ± 0.2. The values are the average of three independent measurements and the error bars represent the standard deviation of the measurements.

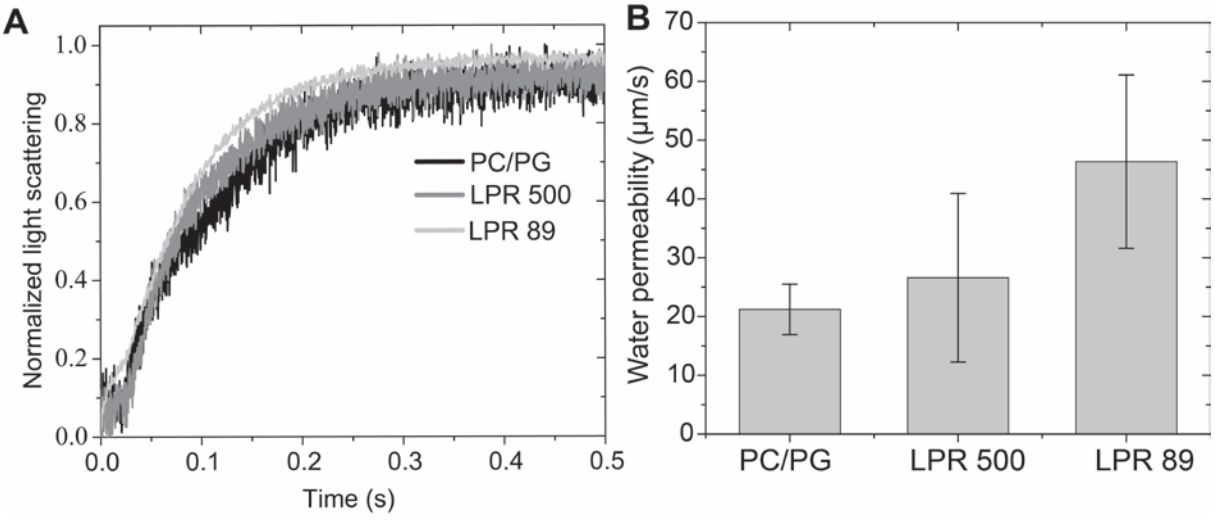

Figure S4. The water permeability of PC/PG (molar ratio of 4:1) vesicles is similar to those of AQP0-containing PC/PG proteoliposomes. A) Stopped-flow light scattering traces obtained with pure PC/PG vesicles (black trace) and AQP0-containing PC/PG proteoliposomes resulting from reconstitution at an LPR of 14.9 (mg/mg; molar LPR of 500) (dark gray trace) or at an LPR of 2.6 (mg/mg; molar LPR of 89) (light gray trace). Due to the low signal-to-noise ratio the three traces are poorly separated, but the noise level is reduced for proteoliposomes reconstituted at an LPR of 2.6. **B)** The water permeability of pure PC/PG vesicles at pH 6.5 was 21.4 ± 4.3 μm/s and that of AQP0 proteoliposomes obtained with a molar LPR of 500 was 26.6 ± 14.3 μm/s, similar to that of the pure lipid vesicles. The water permeability of AQP0 proteoliposomes reconstituted at a molar LPR of 89 was 46.4 ± 14.8 μm/s, corresponding to an increase by a factor of 2.2 ± 0.8 over control liposomes. The values are the average of three independent measurements and the error bars represent the standard deviation of the measurements.

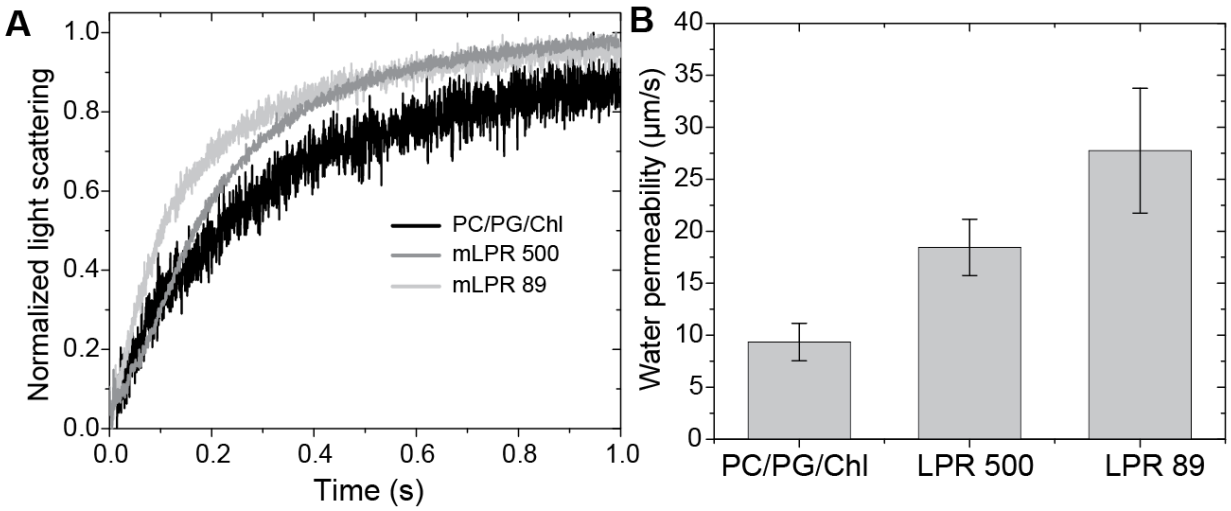

Figure S5. Cholesterol lowers the water permeability of PC/PG/Chl (molar ratio of 2:1:2) control vesicles, making it possible to clearly see the contribution of AQP0 to the water permeability of the vesicles. A) Stopped-flow light scattering traces obtained with PC/PG/Chl vesicles (black trace) and AQP0-containing PC:PG:Chl proteoliposomes resulting from reconstitution at an LPR of 11.9 (mg/mg; molar LPR of 500) (dark gray trace) or at an LPR of 2.1 (mg/mg; molar LPR of 89) (light gray trace). **B)** The water permeability of pure PC/PG/Chl vesicles at pH 6.5 was 9.3 ± 1.8 µm/s. The water permeabilities of AQP0 proteoliposomes reconstituted at molar LPRs of 500 and 89 were 18.4 ± 2.7 µm/s and 27.8 ± 6.0 µm/s, respectively, corresponding to increases by factors of 2.0 ± 0.5 and 3.0 ± 0.9 over control liposomes. The values are the average of three independent measurements and the error bars represent the standard deviation of the measurements.

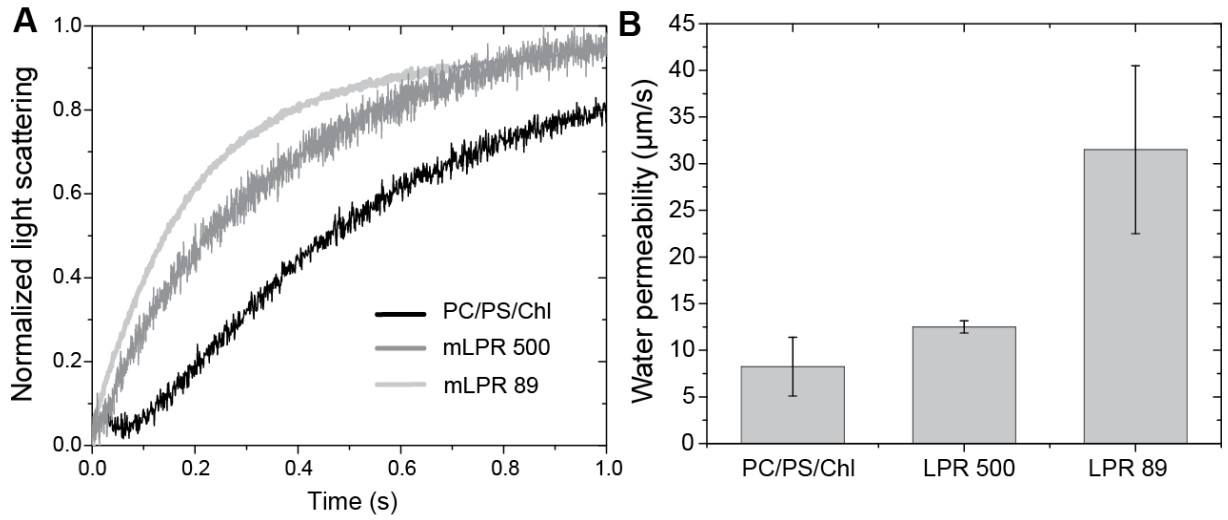

Figure S6. Cholesterol lowers the water permeability of PC:PS:Chl (molar ratio of 4:1:5) control vesicles, making it possible to clearly see the contribution of AQP0 to the water permeability of the vesicles. A) Stopped-flow light scattering traces obtained with PC/PS/Chl vesicles (black trace) and AQP0-containing PC/PS/Chl proteoliposomes resulting from reconstitution at an LPR of 11.2 (mg/mg; molar LPR of 500) (dark gray trace) or at an LPR of 2.0 (mg/mg; molar LPR of 89) (light gray trace). **B)** The water permeability of pure PC/PS/Chl vesicles at pH 6.5 was 8.25 ± 3.2 μm/s. The water permeabilities of AQP0 proteoliposomes reconstituted at molar LPRs of 500 and 89 were 12.5 ± 0.7 μm/s and 31.6 ± 8.9 μm/s, respectively, corresponding to increases by factors of 1.5 ± 0.6 and 3.8 ± 1.8 over control liposomes. The values are the average of three independent measurements and the error bars represent the standard deviation of the measurements.

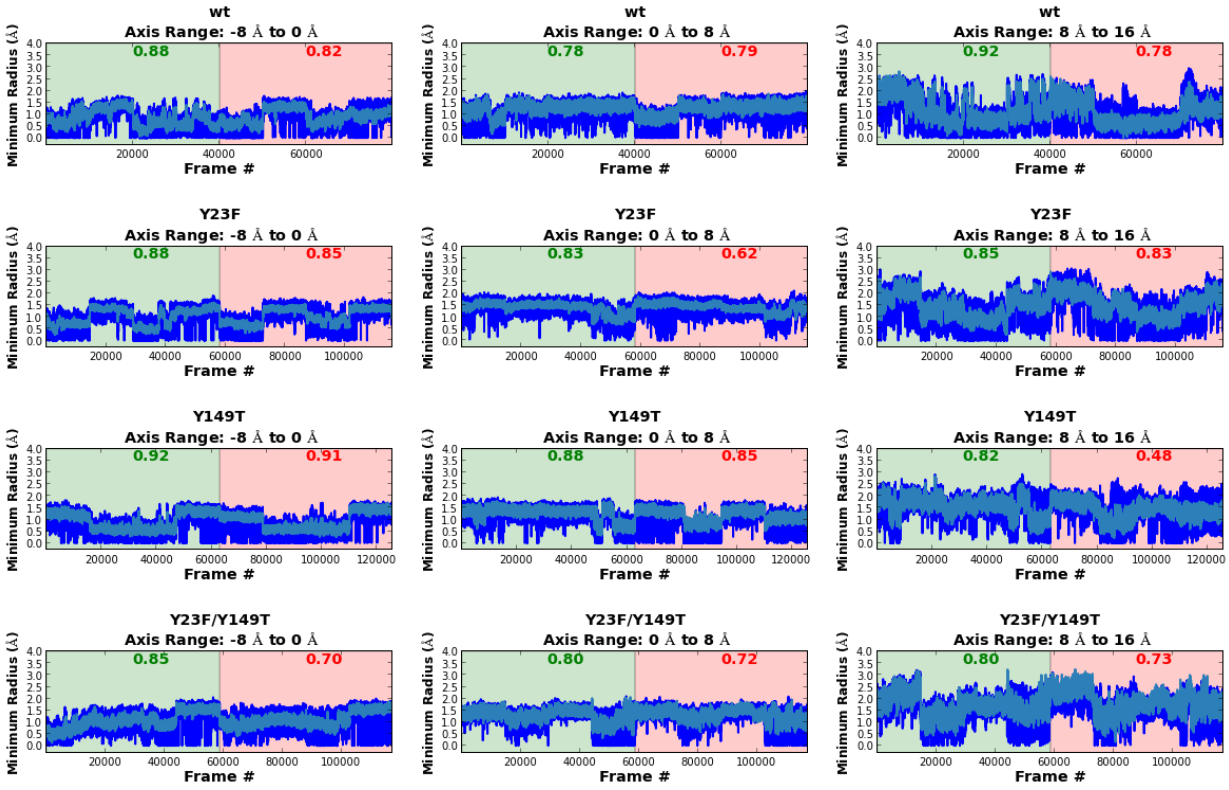

Figure S7. PLS-FMA analysis. Prediction of FMA modes from three sections of the monomer for wild-type AQP0 and the three tyrosine mutants. The training and validation regions are shown in light green and light red, respectively. The corresponding correlation coefficients are given in green and red bold font. The raw simulation data are shown in dark blue and the data modeled from PLS-FMA are shown in light blue.

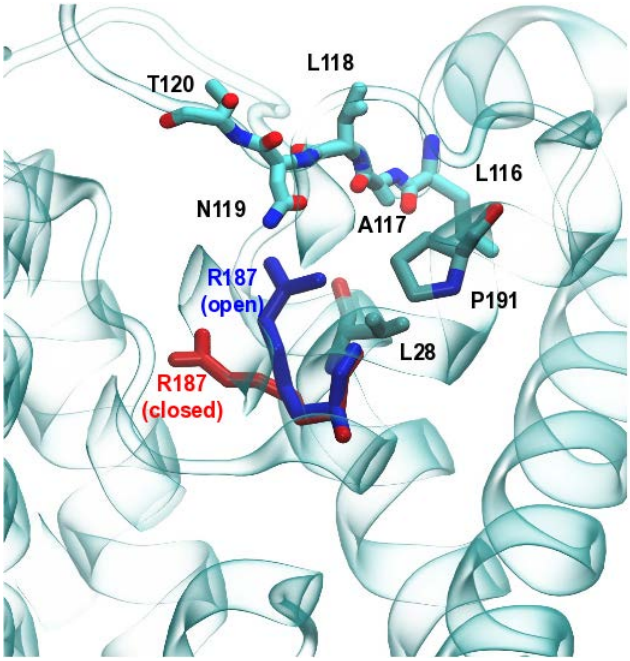

Figure S8. Mutations predicted to stabilize the arginine gate in the open state. The figure shows seven residues that are close to residue Arg-187. Mutations of these residues to either glutamate or aspartate are predicted to stabilize the arginine gate in the open state. These residues, except Pro-191 and Leu-28, are all on extracellular loop C of AQP0.

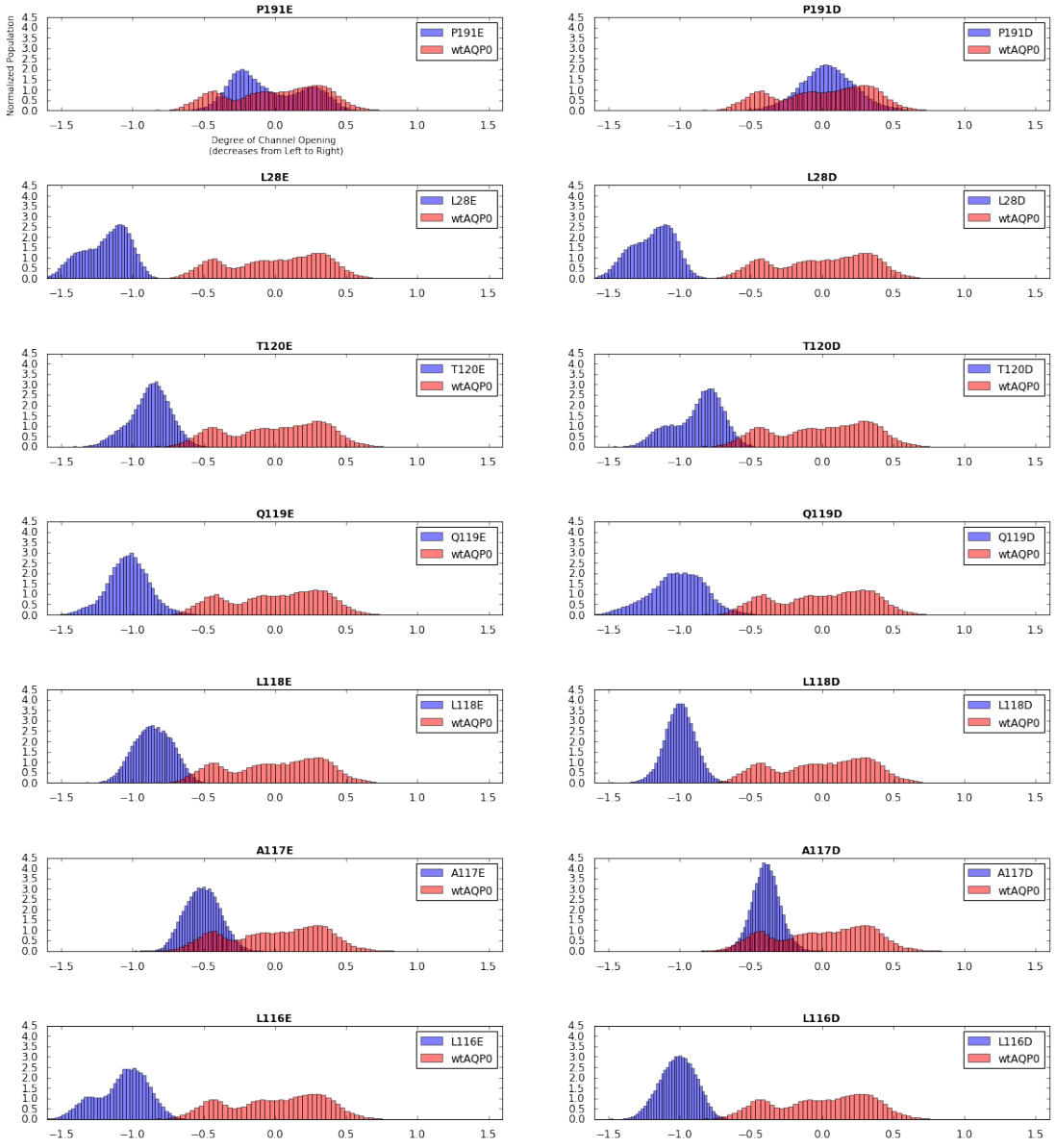

Figure S9. Population distributions of AQP0 proteins with mutations designed to keep the arginine gate in the open state. Except for mutations of Proline-191, the distribution of all investigated mutants is shifted to the right as compared to wild-type AQP0, confirming that the arginine mode remains in the "open" state. The same x-axis "degree of channel opening" applies to each panel.

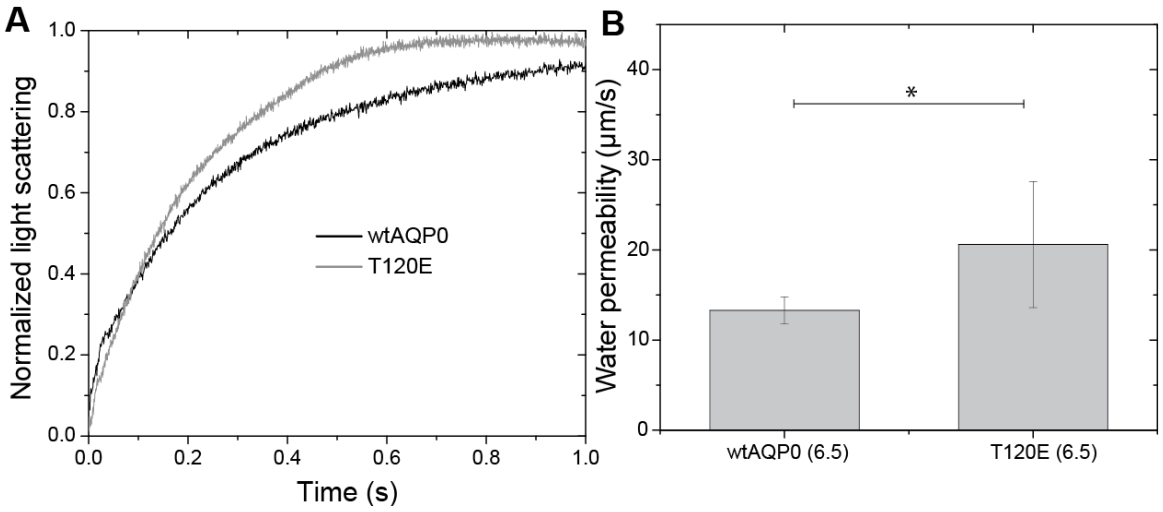

Figure S10. Water permeability of wild-type AQP0 and the T120E mutant reconstituted into PC/PS/Chl vesicles at an LPR 2.0. A) Stopped-flow light scattering traces obtained with wild-type AQP0 (black trace) and the T120E mutant (gray trace). **B)** The water permeability of pure wtAQP0 at pH 6.5 was 13.3 ± 1.5 µm/s and that of the T120E mutant was 20.3 ± 6.5 µm/s. The values are the average of three independent measurements and the error bars represent the standard deviation of the measurements. ANOVA gives a p-value of 0.064, and there is ~93% confidence that the water permeability of the T120E mutant is different from that of wtAQP0.

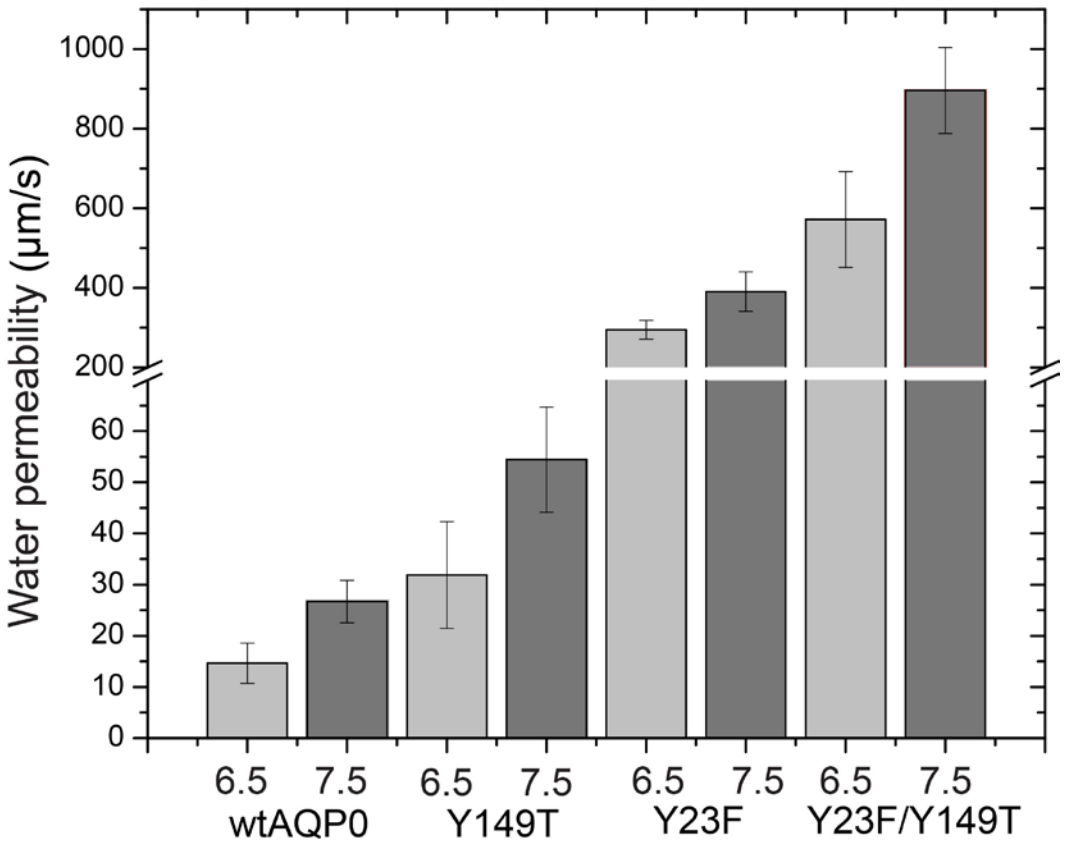

Figure S11. pH sensitivity of wild-type AQP0 and the tyrosine mutants. For wild-type AQP0 and for the Y23F, Y149T and Y23F/Y149T mutants, water permeability is slightly but consistently higher at pH 7.5 than at pH 6.5.

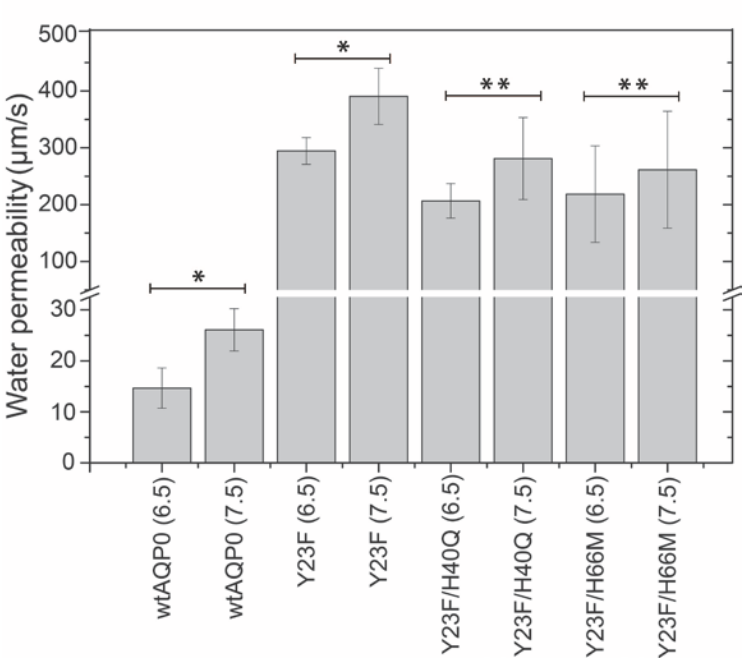

Figure S12. Water permeability at pH 6.5 and 7.5 of wild-type AQP0 and AQP0 mutants in which histidine residues were mutated. Proteoliposomes containing wild-type AQP0 and the Y23F mutant both show statistically significant higher water permeability at pH 7.5 than at pH 6.5 ($p < 0.05$), but differences in permeability were more readily resolved with the Y23F mutant. The water permeability of the H40Q/Y23F was 206.5 ± 30.4 μm/s at pH 6.5 and 281 ± 72 μm/s at pH 7.5, an increase by a factor of 1.4 ± 0.4. The water permeability of the H66M/Y23F was 218.5 ± 85 μm/s at pH 6.5 and 262 ± 103 μm/s at pH 7.5, an increase by a factor of 1.2 ± 0.7. Differences in water permeability at pH 6.5 and 7.5 of the Y23F/H40Q and Y23/H66M double mutants were not statistically significant with a 95% confidence threshold ($p = 0.2$ for Y23F/H40Q and $p = 0.6$ for Y23F/H66M), suggesting that the two histidine residues may have a role in the subtle pH sensitivity of AQP0 water permeability. The error bars represent the standard deviation of the measurement. * $p < 0.05$, ** $p > 0.05$

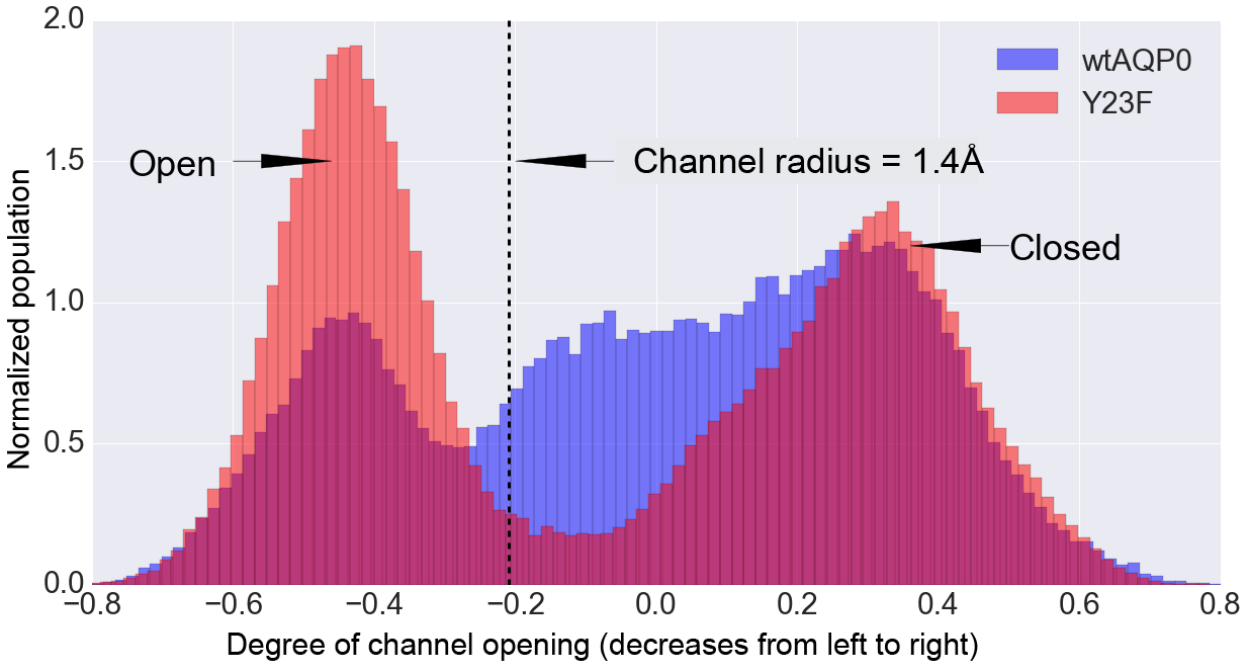

Figure S13. Population distributions along the PLS-FMA modes. Populations of wild-type AQP0 and the Y23F mutant along the arginine gate mode. The Y23F mutant spends almost twice as much time in the open state of the mode as the wild-type protein.

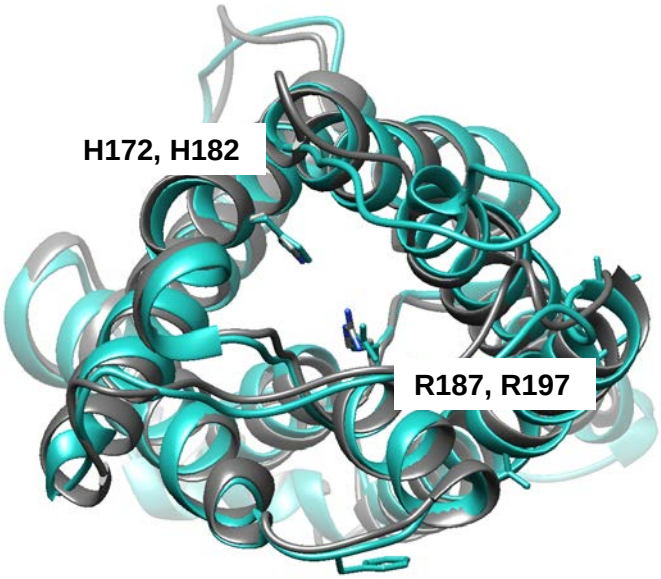

Figure S14. AQP1 (PDB id: 1J4N; light blue) has a histidine residue, His-182, that corresponds to His-172 in AQP0 (PDB id: 2B6O; gray, side chains of residues colored by element). Since AQP1 features a corresponding histidine residue but is not pH-sensitive, His-172 in AQP0 is unlikely to be involved in pH sensitivity. Furthermore, Arg-187 of AQP0 and Arg-197 of AQP1 are in close proximity to His-172 and His-182, respectively. The proximity of the arginine residues to the histidine residues likely shifts the pKa of the histidine residues beyond the physiological range.